

Wang Haitao (Orcid ID: 0000-0001-9900-8528)

Roflupram exerts neuroprotection via activation of CREB/PGC-1 α signaling in experimental models of Parkinson's disease

Running Title: Roflupram protects against Parkinson's disease

Jiahong Zhong^{1,2,#}, Wenli Dong^{1,2,#}, Yunyun Qin^{1,2}, Jinfeng Xie^{1,2}, Jiao Xiao^{1,2}, Jiangping Xu^{1,2,3,4,5*}, Haitao Wang^{1,2,4,5*}

¹ Department of Neuropharmacology and Drug Discovery, School of Pharmaceutical Sciences, Southern Medical University, Guangzhou 510515, China.

² Guangdong Provincial Key Laboratory of New Drug Screening, School of Pharmaceutical Sciences, Southern Medical University, Guangzhou 510515, China.

³ Central Laboratory, Southern Medical University, Guangzhou 510515, China.

⁴ Key Laboratory of Mental Health of the Ministry of Education, Southern Medical University, Guangzhou 510515, China.

⁵ Center for Brain Science and Brain-Inspired Intelligence, Guangdong-Hong Kong-Macao Greater Bay Area.

Equal contribution

*Correspondence:

Prof. Jiangping Xu, M.D., Ph.D.

Tel.: +86-20-61648236, Fax: +86-20-61648236

E-mail: jpx@smu.edu.cn

This article has been accepted for publication and undergone full peer review but has not been through the copyediting, typesetting, pagination and proofreading process which may lead to differences between this version and the Version of Record. Please cite this article as doi: 10.1111/bph.14983

Dr. Haitao Wang, Ph.D.

Tel.: +86-20-61648594, E-mail: wht821@smu.edu.cn

Word count (excluding figure legends and references):

Word count (excluding abstract, methods, figure legends and references):

Acknowledgments:

This work was supported by National Natural Science Foundation of China (No. 81773698), the Program for Changjiang Scholars and Innovative Research Team in University (IRT_16R37), Science and Technology Program of Guangdong (Nos. 2018B030334001 and 2015B020211007), Science and Technology Program of Guangzhou (No. 201604020112).

Conflicts of interest statement:

The authors declare that they have no conflict of interest.

Abstract

Background and Purpose

Roflupram (ROF) improves cognition and limits neuroinflammation in the brain. However, the beneficial effects of ROF in ameliorating Parkinson's disease (PD) remain unknown. Therefore, we aimed to elucidate the pharmacological effects and mechanisms of action of ROF in experimental models of PD.

Experimental Approach

We utilized SH-SY5Y cells exposed to 1-methyl-4-phenylpyridinium iodide (MPP⁺) as an *in vitro* PD model. Cell viability and apoptosis were analyzed via the MTT assay and flow cytometry. Mitochondrial morphology, mitochondrial respiratory capacity and ROS were measured by a mitochondrial tracker, a Seahorse analyzer and a MitoSOX-Red dye. For *in vivo* PD model, behavioral tests, Nissl staining and immunohistochemistry were used to evaluate the protection of ROF. The levels of tyrosine hydroxylase (TH), cAMP response element-binding protein (CREB) and peroxisome proliferator-activated receptor gamma coactivator-1 α (PGC-1 α) were analyzed by Western blotting.

Key Results

ROF decreased MPP⁺-induced apoptosis in SH-SY5Y cells and human dopaminergic neurons. ROF also increased mitochondrial respiratory capacity, decreased ROS production and restored mitochondrial morphology. ROF reversed the MPP⁺-induced reductions of phosphorylated CREB, PGC-1 α , and TH, while the protective effects were blocked by the PKA inhibitor H-89 and via PGC-1 α siRNA. In mice treated with MPTP, ROF significantly improved motor functions. Importantly, ROF prevented both dopaminergic neuronal loss and the reduction of phosphorylated CREB and PGC-1 α in the substantia nigra and striatum.

Conclusion and Implications

ROF protects dopaminergic neurons from apoptosis via the CREB/PGC-1 α pathway in PD models. Hence, ROF has potential as a protective drug for the treatment of PD.

Key words: Parkinson's disease, mitochondria, Phosphodiesterase 4, Roflupram

Abbreviations

CREB, cAMP response element-binding protein;

FCCP, carbonyl cyanide 4-(trifluoromethoxy)phenylhydrazone;

MMP, mitochondrial membrane potential;

MPP⁺, 1-methyl-4-phenylpyridinium iodide;

MTT, 3-(4,5-dimethylthiazol-2-yl)-2,5-diphenyltetrazolium bromide;

MPTP, 1-methyl-4-phenyl-1,2,3,6-tetrahydropyridine;

NC, negative control;

OCR, Oxygen Consumption Rate;

PD, Parkinson's disease;

PDE4, phosphodiesterase 4;

PGC-1 α , peroxisome proliferator-activated receptor gamma coactivator-1 α ;

ROF, roflupram;

Roli, rolipram;

SN, substantia nigra

TMRE, tetramethylrhodamine ethyl ester perchlorate.

Bullet point summary

What is already known

- Roflupram is a PDE4 inhibitor with low emetic potential and excellent blood-brain barrier permeability
- Roflupram reverses cognition deficit in APP/PS1 mice and inhibits neuroinflammation through inducing autophagy

What this study adds

- Roflupram protects dopaminergic neurons from apoptosis and ameliorates motor deficits
- Roflupram improves mitochondrial function through activating CREB and increasing PGC-1 α expression

What is the clinical significance

- Roflupram may be clinically effective in preventing and treating PD

List of Hyperlinks for Crosschecking

| Name | Target ID | Hyperlink |
|------------------|-----------|---|
| PGC-1 α | 593 | https://www.guidetoimmunopharmacology.org/GRAC/ObjectDisplayForward?objectId=593 |
| TH | 1243 | https://www.guidetopharmacology.org/GRAC/ObjectDisplayForward?objectId=1243 |
| CREB | 2734 | https://www.guidetopharmacology.org/GRAC/ObjectDisplayForward?objectId=2734 |
| cAMP | 2352 | https://www.guidetopharmacology.org/GRAC/LigandDisplayForward?ligandId=2352 |
| PKA | 1694 | https://www.guidetopharmacology.org/GRAC/ObjectDisplayForward?objectId=1694&familyId=284&familyType=ENZYME |
| FGF-2 | 4924 | https://www.guidetopharmacology.org/GRAC/LigandDisplayForward?ligandId=4924 |
| GDNF | 4940 | https://www.guidetopharmacology.org/GRAC/LigandDisplayForward?tab=biology&ligandId=4940 |
| Cox2 | 1376 | https://www.guidetopharmacology.org/GRAC/ObjectDisplayForward?objectId=1376 |
| Fasn | 2608 | https://www.guidetopharmacology.org/GRAC/ObjectDisplayForward?objectId=2608 |
| PDE4A | 1300 | https://www.guidetopharmacology.org/GRAC/ObjectDisplayForward?objectId=1300 |
| PDE4B | 1301 | https://www.guidetopharmacology.org/GRAC/ObjectDisplayForward?objectId=1301 |
| PDE4D | 1303 | https://www.guidetopharmacology.org/GRAC/ObjectDisplayForward?objectId=1303 |
| ATP | 1713 | https://www.guidetopharmacology.org/GRAC/LigandDisplayForward?ligandId=1713 |
| H-89 | 5983 | https://www.guidetopharmacology.org/GRAC/LigandDisplayForward?ligandId=5983 |
| levodopa | 3639 | https://www.guidetopharmacology.org/GRAC/LigandDisplayForward?ligandId=3639 |
| MPP ⁺ | 4568 | https://www.guidetopharmacology.org/GRAC/LigandDisplayForward?ligandId=4568 |
| Rolipram | 5260 | https://www.guidetopharmacology.org/GRAC/LigandDisplayForward?ligandId=5260 |
| L-glutamine | 723 | https://www.guidetopharmacology.org/GRAC/LigandDisplayForward?ligandId=723 |

Introduction

Parkinson's disease (PD) is the second most prevalent neurodegenerative disease in the world. The features of PD include: loss of dopaminergic neurons in the substantia nigra (SN), formation of Lewy bodies, overproduction of ROS and mitochondrial dysfunction (Migdalska-Richards *et al.*, 2016). These pathological features lead to clinical manifestations of static tremor, bradykinesia, myotonia and abnormal posture in patients suffering with PD (Jankovic, 2008). Currently available drugs cannot prevent the PD-induced degenerative process of dopaminergic neurons in the SN (Dauer *et al.*, 2003), and they usually produce intolerable side effects. For example, after several years of levodopa therapy, patients become progressively more disabled due to the appearance of motor fluctuations and abnormal involuntary movements (Picconi *et al.*, 2018). Additionally, levodopa may further promote neuronal cell death due to the overproduction of ROS (Kostrzewa *et al.*, 2002). Other drugs, such as dopaminergic agonists, can also produce a range of side effects, including gastrointestinal reactions and psychological effects (Stocchi *et al.*, 2016). Therefore, there are still criticisms and unmet needs for antiparkinsonian therapy. As such, it is necessary to design and discover novel compounds with ideal efficacy and safety to treat PD.

Phosphodiesterase 4 (PDE4) is an enzyme for hydrolyzing cAMP. Inhibition of PDE4 causes an increased level of cAMP, which thereby activates PKA and cAMP response element-binding protein (CREB). CREB is a transcription factor that promotes the transcription of downstream targets, including peroxisome proliferator-activated receptor gamma coactivator-1 α (PGC-1 α) (Wu *et al.*, 2006). We have previously demonstrated a protective role of PDE4 inhibitors in several neurological disease models (Zhong *et al.*, 2018; Zhong *et al.*, 2019). Regarding the role of PDE4 inhibitors in the treatment of PD, it has been reported that inhibition of PDE4 protects dopaminergic neurons and prevents deficits of spatial working memory in patients with PD (Yang *et al.*, 2008; Niccolini *et al.*, 2017), but its mechanism of action remains unclear. Moreover, existing PDE4 inhibitors are mostly limited by their serious side effects, such as nausea and vomiting (Richter *et al.*, 2013). For example, the canonical PDE4 inhibitor rolipram was hindered in phase-II clinical trials for the treatment of depression due to rolipram inducing intolerable nausea and vomiting (Dyke *et al.*, 2002). Roflupram (ROF, also known as ZI-n-91 or FFPM) is a selective PDE4 inhibitor

(Zheng *et al.*, 2008), and its chemical structure is shown in Figure 1A. ROF is a potent PDE4 inhibitor with higher selectivity for PDE4A4, PDE4B2 and PDE4D4 as compared with that for rolipram (Guo *et al.*, 2017). Additionally, ROF penetrates the blood-brain barrier after oral administration, while it induces little or no emetic response (Guo *et al.*, 2017). We have previously found that ROF reverses cognitive deficits in amyloid precursor protein/presenilin 1 (APP/PS1) transgenic mice through activation of the cAMP/PKA/CREB pathway and via suppression of inflammasome activation (Guo *et al.*, 2017; You *et al.*, 2017). These data indicate that ROF has potential for the treatment of neurodegenerative diseases. However, the potential protective efficacy of ROF in PD models is largely unknown.

Activated CREB enhances the expression of PGC-1 α (Herzig *et al.*, 2001). PGC-1 α plays a pivotal role in regulating mitochondrial biogenesis and resistance to ROS (St-Pierre *et al.*, 2006; Ciron *et al.*, 2015), and transgenic mice over-expressing PGC-1 α in dopaminergic neurons are more resistant to neurotoxicity induced by 1-methyl-4-phenyl-1,2,3,6-tetrahydropyridine (MPTP) (Mudo *et al.*, 2012). Inspired by these findings, we sought to determine if ROF could protect dopaminergic neurons against 1-methyl-4-phenylpyridinium iodide (MPP⁺)/MPTP-induced neuronal degeneration, and whether the CREB/PGC-1 α pathway contributes to the protective efficacy of ROF. We found that ROF promoted the survival of SH-SY5Y cells and human dopaminergic neurons subjected to MPP⁺. Moreover, ROF improved behavioral performance and attenuated the loss of dopaminergic neurons in both the SN and striatum of an MPTP-induced mouse model of PD *in vivo*. Mechanistically, the neuroprotective effects of ROF may partly involve the upregulation of the CREB/PGC-1 α pathway. Taken together, we suggest that ROF is a promising compound for preventing the degradation of dopaminergic neurons in patients with PD.

Methods

Animals

Adult male C57BL/6J mice (RRID: IMSR_JAX:000664, 8 weeks old, 22-25 g, specific pathogen free) were obtained from the Laboratory Animal Centre of Southern Medical

University (Guangzhou, China). Mice were housed five per cage (plastic cages) with conventional bedding in the animal facility of Southern Medical University. The mice were adapted to feed for a week before the formal experiments and housed in a standard feeding environment (50%-70% humidity, 23-25°C, 12-12 h light/dark cycle with lights) where could eat and consume water at will. All animal experiments were performed in accordance with the NIH Guide for the Care and Use of Laboratory Animals (NIH, revised 1996), and approved by the Laboratory Animal Ethics Committee of Southern Medical University (Guangzhou, China). All animal studies were performed in compliance with the Animal Research: Reporting of In Vivo Experiments (ARRIVE) guidelines (Kilkenny *et al.*, 2010), and with the implementing guidelines published in the British Journal of Pharmacology (McGrath *et al.*, 2015). Experiments were designed according to the principles of the 3Rs, (replacement, refinement and reduction) to minimize animal pain and reduce the number of mice used in our experiments. Mice were sacrificed after behavioral tests by an overdose of inhaled 5% isoflurane. The sample size calculations were conducted in our pilot study to get the least number of mice needed to detect a significant difference in the level of ATP between MPTP-treated mice and (MPTP+ROF)-treated mice. Using the two-tailed test, a sample size of five mice per group was needed to detect a difference with 95% confidence and 80% power. Based on the power calculation, 10 mice in each group were applied to evaluate the behavioral performance. After behavioral tests, five mice in each group were used for biochemical analysis and the rest mice in each group were used for the immunostaining. No mice were excluded from statistical analysis. A total of 40 mice were used in the experiments described here.

Compounds

ROF (#SML2106) was purchased from Sigma-Aldrich (St. Louis, MO, USA), and the purity was determined to be above 98% by HPLC analysis. Rolipram (#S1403) was obtained from Selleck (Houston, TX, USA), and the purity was determined to be above 98% by HPLC analysis. For *in vitro* experiments, ROF was dissolved in DMEM/F12 medium containing 0.1% DMSO. In animal experiments, ROF and rolipram were suspended in vehicle (6% Solutol HS-15, 1% DMSO, 40% Hydroxypropyl- β -Cyclodextrin) to obtained working solutions.

Experimental design for MPTP mouse model of PD

Mice were randomly divided into four groups (10 mice per group). On the first day of the experiment, the mice in the vehicle group and the MPTP group were given solvent (i.g.) at 100 g·mL⁻¹, and the other two groups were given ROF (1.0 mg·kg⁻¹, i.g.) and rolipram (2.5 mg·kg⁻¹, i.g.) at 100 g·mL⁻¹, respectively. On the second day, 2 h after ROF and rolipram were orally administration, the mice in the vehicle group were given saline (i.p.) at 100 g·mL⁻¹, and the other three groups were given MPTP (30 mg·kg⁻¹, i.p.) at 100 g·mL⁻¹. The experimental operation in next four days was the same as the second day. Starting on the seventh day of the experiment, all mice were reared under normal condition for 10 days, during which behavioral experiments were performed and corresponding tissues were extracted. This model of PD in mice replicates biochemical and histological changes in humans suffering from PD (Heikkila *et al.*, 1984).

Cell culture

SH-SY5Y cell line used in our experiments was derived from American Type Culture Collection (ATCC, Cat#CRL-2266, RRID: CVCL_0019). Cells were cultured in culture flask containing 5 mL of culture medium, and the culture medium included Nutrient Mixture Ham's F-12 with 1% penicillin/streptomycin and 10% (v/v) FBS. The culture condition of incubator was 95% air and 5% CO₂ at 37°C and cells were passaged at 48 h per interval.

Lund Human Mesencephalic (LUHMES) cell line used in our study was derived from American Type Culture Collection (ATCC, Cat#CRL-2927, RRID: CVCL_B056). The cell culture and differentiation protocol have been described previously (Scholz *et al.*, 2011; Schildknecht *et al.*, 2013). Briefly, conditionally immortalized cells were cultured and maintained in DMEM/F12 supplemented with N2 supplement, 2 mM L-glutamine and 40 ng/ml fibroblast growth factor 2 (FGF-2) at 37°C with 5% CO₂. For differentiation, cells were seeded in culture flask pre-coated with 1 µg/ml fibronectin and 50 µg/ml poly-L-ornithine (PLO) in proliferation medium. After 24 h, the medium was replaced with differentiation medium, composed of advanced DMEM/F12 with N2 supplement, 2 mM L-glutamine, 2.25 µM tetracycline, 2 ng/ml recombinant human glial cell-derived neurotrophic factor and 1 mM dibutyryl 3',5'- cAMP. During the process of cell differentiation, medium was changed with

fresh differentiation medium every other day. After 6 days of differentiation, LUHMES cells are characterized by high expression of TH, and used as a human dopaminergic neurons (Scholz *et al.*, 2011; Krug *et al.*, 2014).

Cell viability assay

SH-SY5Y cells were cultured in 96-well plates at 1×10^4 cells per well overnight at 37°C with 95% air and 5% CO₂. Then, the cell culture solution was discarded, and the culture medium containing different concentrations of ROF was added to each well for 1 h incubation. The concentrations of ROF were used are reported in the figure legends. Subsequently, cells were exposed to 500 μM of MPP⁺ for 48 h. Ultimately, the culture medium was discarded, and MTT solution (0.5 mg·mL⁻¹) was added to each well for 4 h. After the MTT solution was replaced with 150 μL of DMSO, the mixture was shaken for 10 min and was then subjected to absorbance detection at a wavelength of 570 nm in a microplate reader (Synergy HT; BIOTEK, Broadview, IL).

LDH assay

SH-SY5Y cells were cultured in 96-well plates at 1×10^4 cells per well overnight. Cells were pretreated with ROF for 1 h, and then were exposed to 500 μM of MPP⁺ for 48 h, the 96-well plates were centrifuged for 5 min in a plate centrifuge at 400 g. Then, 120 μL of the supernatant from each well was transferred to a new 96-well plate. The prepared LDH working solution was added to 96-well plates according to the standard of 60 μL per well, and it was then mixed at room temperature for 30 min in the dark. Eventually, the liquid absorbance values in the wells were measured at both 490 nm and 600 nm.

Flow cytometric analysis of apoptosis

SH-SY5Y cells were cultured in 6-well plates at 2×10^5 cells per well and were incubated overnight. Then, the culture medium was discarded, and the medium containing different concentrations of ROF was added for a 1 h incubation. The concentrations of ROF were used are reported in the figure legends. Subsequently, cells were exposed to 500 μM of MPP⁺ for 24 h. The cell supernatant was then removed, and the cells were digested and centrifuged at 1000 rpm for 5 min. Then, 500 μL of binding buffer and 5 μL of Annexin-V-FITC were

mixed and added to the centrifuge tube; subsequently, 5 μL of PI was also mixed into the centrifuge tube. Finally, these samples were then subjected to flow cytometry (BD FACS-Verse™ Flow Cytometer, BD Biosciences, San Jose, CA, USA).

ATP analysis

Cells were cultured in 6-well plates at 2×10^5 cells per well overnight. Cells were then treated with ROF and MPP⁺ for 24 h. Then, cells were lysed in lysis buffer for 10 min, and centrifuged at 12,000 g for 5 min at 4°C. The supernatant was collected for subsequent measurement. 100 μL of ATP detection solution was added to the detection well and placed at room temperature for 5 min so that all the background ATP was consumed. Eventually, 20 μL samples were added to each well and quickly mixed with a micro liquid shifter. The RLU value was then determined by chemiluminescence instrument (luminometer). The protein concentration of the sample was determined by BCA protein assay kit. The relative ATP level was calculated as following formula: relative ATP level = ATP value/protein value.

Mitochondrial membrane potential (MMP) measurement

SH-SY5Y cells were cultured in confocal dishes at a density of 1×10^5 cells·mL⁻¹. The next day, cells were treated ROF (20 μM) 1 h before incubation with 500 μM of MPP⁺ for 24 h. After the cells were treated, the culture medium was discarded and cells were washed three times with PBS for 5 min each time. The tetramethylrhodamine ethyl ester perchlorate (TMRE) (50 nM) dye was added to the confocal dishes, incubated for 20 min without light, and then washed with three times PBS for 5 min each time. Finally, the confocal dishes were placed in an inverted confocal microscope (ECLIPSE Ti, Nikon, Tokyo, Japan) for imaging.

Determination of ROS

SH-SY5Y cells were cultured in 24-well plates at a density of 1.2×10^5 cells·mL⁻¹ and were allowed to adhere overnight. After treatment with 20 μM of ROF and 500 μM of MPP⁺ for 24 h, the cells were washed three times with PBS for 5 min each time. MitoSOX-Red (2 μM) dye was added to each well, incubated for 1 h without light at 37°C, and was then washed three times with PBS for 5 min each time. Finally, the plates were placed under a fluorescent microscope (ECLIPSE Ti-U, Nikon, Tokyo, Japan) for imaging.

Immunostaining

SH-SY5Y cells were seeded in confocal dishes at a density of 1.2×10^5 cells·mL⁻¹. Then, the cells pretreated with ROF (20 μM) were incubated with 500 μM of MPP⁺ for 48 h. Subsequently, after washing with PBS for 5 min each time. 300 μL of 4% paraformaldehyde was added to each dish for 20 min at 37°C and the dishes were then washed three times with PBS. Then, 300 μL of 0.2% Triton X-100 was added to each dish for 10 min at room temperature and then was washed three times with PBS for 5 min each time. Cells were then incubated in 300 μL of 5% BSA solution (in PBS) for 50 min at room temperature; then, cells were incubated with anti-cleaved caspase-3 antibody solution (1:200) overnight at 4°C. On the next day, the wells of the confocal dishes were washed three times with PBS for 5 min each time. After the washed PBS was discarded, the secondary antibody solution (1:200) was added and incubated for 4 h in the dark at 4°C. After incubation, the secondary antibody was removed and samples were then washed three times with PBS for 5 min each time. Subsequently, Hoechst 33342 (2 μg·mL⁻¹) was incubated in the dishes for 15 min, washed with PBS and samples were then examined under an inverted confocal microscope.

Transfection of small interfering RNA (siRNA)

Specific siRNA for PGC-1α (siPGC-1α) were obtained from Shanghai GenePharma Co (Shanghai, China). The sequences were as follows: sense: 5'-GGCACGCAAUCCUAUUCATT-3'; antisense: 5'-AUGAAUAGGAUUGCGUGCCTT-3'. Scrambled siRNA sequences was used as the negative control (NC). The SH-SY5Y cells were cultured in 6-well plates at a density of 1×10^5 cells·mL⁻¹ and allowed to adhere overnight. According to the manufacturer's instructions, Lipofectamine 2000 (Invitrogen, Carlsbad, CA, USA) was mixed with Opti-MEM and mixed with siRNA (50 nM) for 20 min. Then, the mixture was added to each well. 6 h after transfection, culture medium was removed and replaced with fresh medium. Cells were used for further analysis 24 hours after transfection.

Analysis of mitochondrial morphology

Cells were cultured in confocal dishes at a density of 1.2×10^5 cells·mL⁻¹ and were allowed to adhere overnight. After treatment with ROF and 500 μM of MPP⁺ for 24 h, the culture

medium was discarded and cells were washed three times with PBS for 5 min each time. Subsequently, Mitotracker Red (500 nM) dye was added to each dish, incubated for 1 h without light at 37°C, and then washed with PBS three times for 5 min each time. Finally, the confocal dishes were placed under an inverted confocal microscope for observation and image capturing, and the images were analyzed using an image analysis system (Image-Pro Plus, version 6.0) with the Mitochondrial Network Analysis (MiNA) toolset. MiNA is freely available at <https://github.com/ScienceToolkit/MiNA>. The analysis and statistics of the mitochondrial captured images were performed according to a previously published article (Valente *et al.*, 2017).

Western blotting

Brian tissues were subjected to ultrasound in RIPA buffer supplemented with a protease- and phosphatase inhibitor cocktail (Sigma-Aldrich). Samples were then centrifuged at 12,000 rpm for 15 min at 4°C, after which the supernatant was extracted. According to the manufacturer's instructions, protein quantification was performed using the BCA a protein assay, and then the prepared protein was boiled at 95°C for 10 min, and 20 µL of each tube was used to load 40 µg of protein for electrophoresis in 10% SDS-PAGE. After electrophoresis, the protein was transferred to PVDF membranes (Millipore, #ISEQ00010); transferring was performed under constant pressure at 86 V for 90 min. Subsequently, 5% non-fat dry milk prepared with TBST was used for blocking at room temperature for 2 h. Subsequently, the membranes were washed four times for 5 min each time with TBST and the primary antibodies were incubated at 4°C overnight. Then, the membranes were washed four times for 5 min each time with TBST and the secondary antibodies were incubated at 4°C for 4 h. Finally, the membranes were washed four times for 5 min each time, and chemiluminescent reagent was added dropwise for exposure. The gray value of the protein in the exposed membranes were analyzed by image analysis system (Image-Pro Plus, version 6.0).

Measurement of Mitochondrial Respiratory Capacity

Mitochondrial respiratory capacity of SH-SY5Y cells was detected using a Seahorse XF-24 Analyzer (Seahorse Bioscience, Billerica, MA, USA) by measuring the oxygen consumption

rate (OCR). Cells were treated as the manufacturer's recommended protocol. Briefly, the OCR was measured by the sequential addition of oligomycin (an ATP synthase inhibitor, 1 μ M), phenylhydrazine (FCCP, a mitochondrial respiration uncoupler, 0.5 μ M) and rotenone (a complete respiratory inhibitor, 2 μ M). This protocol is normally used for the determination of basal OCR, ATP-linked respiration and maximal respiration (Tomkova *et al.*, 2018). After the measurement of mitochondrial respiratory capacity, cells were lysed and the total protein was quantified using the BCA a protein assay. Final result was normalized with protein content of the corresponding well.

Real-time PCR for mtDNA Copy Number Analysis

Total DNA was extracted from SH-SY5Y cells using TIANamp Genomic DNA Kit (TIANGEN BIOTECH, Beijing, China). Real-time PCR analysis using LC480 SYBR Green I Master (Roche, Basel, Switzerland) was performed on a real-time PCR system (Roche, Basel, Switzerland). The ratio of mitochondria DNA (mtDNA, represented by the Cox2) to nuclear DNA (represented by the Fasn) was shown as relative mtDNA copy number. The primers for the Cox2 gene were: Cox2-forward, 5'-CAGTCCCCTCCCTAGGACTT-3'; Cox2-reverse, 5'-TTTCAGAG CATTGGCCATAGAA-3'. The primers for the Fasn gene were: Fasn-forward, 5'- AGGATATGGAGAGGGCTGGT-3'; Fasn-reverse, 5'-ACCCAAGCATCATTTTCGTC-3'.

Polo test

The mice were acclimated for 30 min in the behavioral testing laboratory before the experiment. A straight wood rod with a diameter of 0.8 cm and a height of 60 cm was used. There was a small wooden ball at the top of the rod, which was covered with gauze to prevent the mouse from slipping. Mice were placed on top of the straight rod and we recorded the time that the mice climbed along the wood to the bottom of the rod. Mice were trained for two days before formal behavioral testing. Each training session consisted of three trials.

Rotarod test

Mice were trained for three days prior to formal testing. Mice were placed on a rotarod at a speed of 20 rpm from slow to fast, and they were able to learn to walk freely within 5 min,

after which the training was over. At the time of the formal experiment, the mice were placed on a rotarod with a rolling speed of 12 rpm, and the duration that the mice stayed on the rotarod were observed and recorded.

Gait Dynamics

Gait dynamic analysis is a well established method to monitor motor defects in MPTP-treated mice (Amende *et al.*, 2005). In the present study, two days before the formal behavioral test, mice were trained daily and placed on a running belt at a speed of 20 cm·s⁻¹ for approximately 30 s. When the mice were able to walk smoothly on the treadmill belt, they were removed and the training was over. When the mice were formally tested for behavior, the mice were placed in a walking compartment with a width of 7 cm and a length of 30 cm. The gait analysis system continuously imaged the underside of the mice. The mice walked for about 5 s on the transparent treadmill belt at a speed of 30 cm·s⁻¹. A video of stable walking of each mouse was analyzed by gait software system (DigiGait Analysis Software Version 14.5). The parameters of stride length, stride duration, ataxia coefficient, and stride frequency of the limbs of the mice were obtained and analyzed as previously described (Goldberg *et al.*, 2011).

Nissl staining

Brains were removed from paraformaldehyde for paraffin embedding, and brain sections with the striatum and SN were sliced to a thickness of 4 μm. The paraffin sections were dewaxed, washed with water, stained in toluidine blue dye solution for 5 min, washed with water and were then baked. The sections were cleaned with xylene and sealed with neutral gum. Slices were placed under a microscope for observation and imaging. Nissl-positive neurons in the SN and striatum regions were counted.

Immunohistochemistry

Paraffin sections of the SN and striatum were deparaffinized, washed with water, and subjected to antigen retrieval using citrate antigen repair buffer (pH 6.0). The sections were placed in 3% hydrogen peroxide solution, and incubated at room temperature for 25 min in the dark. After which they were washed three times for 5 min each time on a decolorizing

shaker. The tissue was evenly covered with 3% BSA dropwise in the culture circle and was incubated at room temperature for 30 min. The blocking solution was gently removed, and an anti-tyrosine hydroxylase (TH) primary antibody solution was added dropwise to the sections, and the sections were placed in a wet box and incubated at 4°C overnight. The slides were placed in PBS (pH 7.4) and washed three times on a decolorizing shaker for 5 min each wash. After the sections were dried, the secondary antibody covered with the corresponding species of the primary antibody was added dropwise and incubated for 50 min at room temperature. After the slices were subjected to 3,3'-diaminobenzidine (DAB) development, the sheets were dehydrated. Positive antibody expression in the sections was dark brown, and images were collected under a microscope. Numbers of TH-immunoreactive neurons were counted in the SN and the intensity of dopaminergic neuron fibers in the striatum were quantified using Image J, respectively.

Immunofluorescent staining

Brains were removed from 30% sucrose for frozen sectioning of the SN and striatum, and the sections were washed three times with 1× TBS for 10 min each wash. Then, 5% goat serum containing 0.3% Triton 100-X TBST was used for blocking for 1 h at room temperature, and sections were incubated overnight at 4°C in a dilution of the primary antibody. The sections were washed three times with TBST, and the secondary antibody solution was incubated in the dark for 1 h at room temperature. The sections were then washed three times with TBST for 10 min each time. Hoechst 33342 (2 µg·mL⁻¹) was added for staining, and the mixture was allowed to stand at room temperature for 15 min. Finally, the sections were washed three times with TBST for 10 min each time. The tissue sections were attached to glass slides, mounted with mounting medium, and after waiting for the mounting medium to solidify were placed under a microscope for observation and imaging.

Data and Statistical Analysis

The data and statistical analysis comply with the recommendations on experimental design and analysis in pharmacology (Curtis *et al.*, 2018). For all studies, experimenters were blind to the specific groups, the treatment conditions, and treatments of the trained/tested mice.

Quantitative analysis of fluorescence optical density values and protein expression normalized to the mean of the control group or negative control group for unwanted sources of variation. The bands used for statistical analysis in Western blot were normalized to GAPDH or total protein. The data in the paper are presented as mean \pm SD, and the n represents the number of animals or tissue samples or cell preparations. Statistical comparison calculations were performed using SPSS 19.0 software. Each experiment was performed independently five times. Statistical significance analysis was performed using one-way analysis of variance (ANOVA) and Bonferroni *post hoc test* when F achieved $P < 0.05$ and there was no significant variance inhomogeneity. When $P < 0.05$ was considered statistically significant difference.

Materials

Dimethylsulfoxide (DMSO) (#D2650), 1-Methyl-4-phenylpyridine iodide (MPP⁺) (#D048) and 3-(4,5-dimethyl-2-thiazolyl)-2,5-diphenyl-2-H-tetrazolium bromide (MTT) (#M2128) were bought from Sigma-Aldrich (St. Louis, MO, USA). Cell counting kit-8 (CCK-8) (#CK04) was obtained from Dojindo Corporation (Tokyo, Japan). Oligomycin (#495455), carbonyl cyanide 4-(trifluoromethoxy)phenylhydrazone (FCCP) (#C2920), poly-L-ornithine (#P3655), fibronectin human plasma (#F0895) and rotenone (#R8875) were bought from Sigma-Aldrich (St. Louis, MO, USA). 1-Methyl-4-pheynl-1,2,3,6-tetrahydropyridine (MPTP) hydrochloride (#S4732) and H-89 (#S1582) were purchased from Selleck (Houston, TX, USA). Tetramethylrhodamine, Ethyl Ester, Perchlorate (TMRE) (#T669), MitoSOX Red (#M36008) and Hoechst 33342 (#H1399) were obtained from Thermo Fisher Scientific, Inc. (Waltham, MA, USA). Annexin V-FITC/PI double staining cell apoptosis detection kit (#KGA108) was purchased from KeyGen Biotech (Nanjing, China). LDH Cytotoxicity Assay Kit (#C0017) and ATP Assay Kit (#S0026) were obtained from Beyotime Institute of Biotechnology (Shanghai, China). BCA protein assay kit (#23225) and Mitotracker Red (#M7512) were bought from Thermo Fisher Scientific, Inc. (Waltham, MA, USA). Culture medium, fetal bovine serum (FBS) (#10099141) and Phosphate Buffered Saline (PBS) (#10010023) were purchased from Gibco (Carlsbad, CA, USA). TIANamp Genomic DNA Kit (#DP304) was obtained from TIANGEN BIOTECH (Beijing, China). LC480 SYBR

GreenIMaster (#4887352001) was purchased from Roche (Basel, Switzerland). Anti-GAPDH (#2118, RRID: AB_561053) and anti-cleaved caspase-3 (#9661S, RRID: AB_2341188) were bought from Cell Signaling Technology (Danvers, USA). Anti-TH (#ab152, RRID: AB_390204), anti-p-CREB (Ser133, #06-519, RRID: AB_310153) and anti-T-CREB (#AB3006, RRID: AB_91283) were obtained from Merck-Calbiochem (St. Louis, MO, USA). Anti-PGC-1 α (#ab54481, RRID: AB_881987) was purchased from Abcam (Cambridge, MA, USA). Lipofectamine 2000 (#11668019) and lipofectamine 3000 (#L3000015) were the products from Invitrogen (Invitrogen, Carlsbad, CA, USA).

Nomenclature of targets and ligands

Key protein targets and ligands in this article are hyperlinked to corresponding entries in <http://www.guidetopharmacology.org>, the common portal for data from the IUPHAR/BPS Guide to PHARMACOLOGY (Harding *et al.*, 2018), and are permanently archived in the Concise Guide to PHARMACOLOGY 2017/18 (Alexander *et al.*, 2017).

Results

ROF increases cell viability and protects against apoptosis in SH-SY5Y cells exposed to MPP⁺

To investigate whether ROF would produce a potential protective effect in dopaminergic cells, we first treated SH-SY5Y cells with ROF alone for 48 h and detected cell viability using a MTT assay. We found that treatment with ROF (2.5–40 μ M) alone had no effect on cell viability (Figure 1B). We then investigated the protective effect of ROF. As shown in Figure 1C, MPP⁺ significantly reduced cell viability, while ROF reversed the impairment mediated by MPP⁺ and increased cell viability in a concentration-dependent manner. The results from the flow cytometry assay showed that MPP⁺ enhanced apoptosis significantly, while ROF reduced the ratio of apoptotic cells at both early and late stages of apoptosis (Figure 1D and E). To further verify the protective effect of ROF, we analyzed the activity of LDH released in the culture medium. We found that LDH activity was markedly enhanced by exposure with MPP⁺. As expected, this increase was remarkably blocked by ROF (Figure 1F). Cytochemical

staining for cleaved caspase-3 was also performed to examine the cellular apoptosis. Consistently, ROF decreased the expression of cleaved caspase-3 in a dose-dependent manner (Supplementary Fig. S1). These results suggest that ROF is highly neuroprotective against MPP⁺ in SH-SY5Y cells.

ROF reverses mitochondrial damage induced by MPP⁺

Our previous studies indicate that inhibition of PDE4 in SH-SY5Y cells reduces the level of ROS (Zhong *et al.*, 2019). As mitochondria are the major organelle producing ROS inside cells, we next investigated whether ROF affected the morphology and functions of mitochondria. A specific mitochondrial tracker was used to assess morphology (Figure 2A). The numbers of networks/individuals, mitochondrial fluorescence intensity, mitochondrial footprints and number of mitochondria were analyzed (Figure 2B–F), MPP⁺ treatment destroyed the mitochondrial network and caused a decrease in the absolute number of networks per cell. Treatment with ROF (20 μM) increased the number of networks (Figure 2B). Mitochondrial-related indicators such as the number of individuals, mitochondrial fluorescence intensity, mitochondrial footprint and number of mitochondria also decreased. After treatment with ROF (20 μM) for 24 h, the above mitochondrial morphological parameters were increased (Figure 2C, D, E and F). To investigate the role of ROF on the alteration of MMP, cells were stained with a TMRE fluorescent dye. As shown in Figure 2G and H, pretreatment with ROF attenuated the loss of MMP. We then measured the production of ROS originating from mitochondria (mtROS). As shown in Figure 2I and J, ROF decreased the MitoSOX fluorescence remarkably in the presence of MPP⁺. We also measured the levels of ATP and mtDNA in cells. The results showed that pretreatment with ROF antagonized the role of MPP⁺ and increased the levels of both mtDNA and ATP (Figure 2K–L). Similarly, treatment with ROF significantly increased basal and maximum mitochondrial respiration in SH-SY5Y cells challenged with MPP⁺ (Figure 2M–N), suggesting that ROF increased the oxidative capacity of mitochondria. These data indicate that ROF attenuates MPP⁺-induced impairment and ameliorates both the morphology and function of mitochondria.

ROF enhances the level of phosphorylated CREB and the expression of PGC-1 α

Our previous studies have shown that inhibition of PDE4 in neuronal cells increases the level of cAMP and thereby activates the PKA/CREB signaling pathway (Guo *et al.*, 2017; Zhong *et al.*, 2018). PGC-1 α is a target of CREB and is a key factor in regulating the biogenesis and function of mitochondria (Herzig *et al.*, 2001; Ciron *et al.*, 2015). Thus, we were interested in investigating whether ROF plays its protective role via CREB/PGC-1 α signaling. As shown in Figure 3A, we found that MPP⁺ decreased the protein expression of TH in SH-SY5Y cells, and that ROF counteracted the role of MPP⁺. We then found that the level of phosphorylated CREB was significantly decreased in response to MPP⁺ stimulation, as compared to that of the control. Additionally, the phosphorylation of CREB was increased as result of ROF treatment (Figure 3C and D). Similar results were observed in terms of the protein level of PGC-1 α (Figure 3E and F). These data suggest that ROF normalized CREB activation and increased PGC-1 α expression to ameliorate MPTP-induced cellular deficits.

Activation of PKA/CREB/PGC-1 α signaling is essential for ROF-mediated neuroprotection against MPP⁺-mediated cellular damage

To investigate the involved signaling pathway responsible for the protective effect of ROF, SH-SY5Y cells were pretreated with the PKA inhibitor, H-89, for 1 h, and were then exposed to MPP⁺ in the presence of ROF. As shown in Figure 4A, ROF reversed the MPP⁺-induced reduction of phosphorylated CREB and PGC-1 α , while H-89 significantly blocked the stimulatory role of ROF on the expression of PGC-1 α and phosphorylation of CREB (Figure 4A–C). We then asked whether PKA/CREB and PGC-1 α mediate the neuroprotective effects of ROF. As shown in Figure 4D and E, ROF reversed the inhibitory role of MPP⁺ on MMP, while H-89 blocked the stimulatory role of ROF on MMP. Simultaneously, we determined cell viability using a LDH assay. We found that H-89 alone had no toxic effect in SH-SY5Y cells, whereas it blocked the protective effects of ROF and decreased LDH release (Figure 4F). We then determined the involvement of PGC-1 α . Cells were transfected with PGC-1 α specific small-interfering RNA (siRNA) or a negative control (NC). The knock-down efficiency was confirmed by Western blot (Supplementary Fig. S2). Our results showed that knocking down PGC-1 α attenuated the role of ROF on MMP (Figure 4G and H). In

accordance with this finding, knocking down PGC-1 α abolished the protective effect of ROF (Figure 4I). We then performed a rescue experiment with over-expression of PGC-1 α in SH-SY5Y cells. A PGC-1 α plasmid was transfected into the siRNA-treated SH-SY5Y cells. We found that over-expression of PGC-1 α reversed the reduction of the MMP induced by MPP⁺ and PGC-1 α siRNA (Figure 4J–L). Taken together, these data support that ROF protects SH-SY5Y cells against MPP⁺-induced neuronal cell injury through activation of the PKA/CREB/PGC-1 α pathway.

ROF shows neuroprotection against MPP⁺-mediated cellular damage in human dopaminergic neurons

We then investigated whether ROF exerts similar effects in human dopaminergic neurons. We took advantage of LUHMES cells. These are conditionally immortalized mesencephalic neuronal precursors that can be differentiated to fully postmitotic human dopaminergic neurons (Efremova et al., 2015). After 6 days of differentiation, we found that TH was robustly expressed in human dopaminergic neurons (Figure 5A–B). We then found that ROF (5–40 μ M) did not affect the neuronal cell viability (Figure 5C). As shown in Supplementary Figure S3, MPP⁺-induced a comparable level of toxicity at 5 μ M (56% cell viability reduction). Therefore, we used this concentration to test the neuroprotection of ROF with this toxin. We found that ROF significantly protected human dopaminergic neurons from MPP⁺-induced toxicity, as evidenced by decreased LDH release and increased cell viability and ATP production (Fig. 5D–F). The results confirm the similar protective effects of ROF in human dopaminergic neurons.

ROF improves motor deficits in MPTP-treated mice

We next investigated the protective effects of ROF in a mouse model of PD. Canonical PDE4 inhibitor rolipram was used as a positive control. The experimental timeline is shown in Figure 6A. In the Pole test, compared with that of mice in the vehicle group, mice in the MPTP-treated group spent much more time to turn downward and climb from the top of the pole to the bottom. Treatment with ROF and rolipram ameliorated motor deficits (Figure 6B). Representative pole test videos of MPTP-treated mice with and without ROF treatment is

shown in Supplementary Movie S1. Similarly, in the rotarod test, mice treated with ROF or rolipram spent significantly longer time on the rotarod compared to that of mice injected with MPTP alone (Figure 6C, Supplementary Movie S2). Additionally, we used a gait dynamic-analysis system to investigate the effects of ROF treatment on limb coordination and motor coordination in MPTP-induced mice (Supplementary Movie S3). As shown in Figure 6D–G, the length of one paw across the given stride was defined as the stride length, which was significantly shorter in MPTP-treated mice compared to that of vehicle-treated mice, and it was increased after administration of ROF and rolipram, indicating an increase in gait stability (Figure 6D). The stride frequency was determined by measuring the number of complete steps per paw per second, which was increased in the MPTP-treated mice, and was decreased after treatment both with either ROF or rolipram (Figure 6E). The ataxia coefficient was increased in MPTP-induced mice, indicating an increase in gait instability compared to that of vehicle-treated mice. Both ROF and rolipram ameliorated gait inconsistency caused by MPTP (Figure 6F). Similarly, both ROF and rolipram treatments alleviated the reduction in stride duration in MPTP-treated mice (Figure 6G). These results indicate that both ROF and rolipram treatments improved limb coordination and motor coordination in MPTP-treated mice.

ROF promotes dopaminergic neuronal survival in both the SN and striatum in MPTP-treated mice

Next, we explored whether the neuroprotective effect of ROF was associated with a decreased loss of dopaminergic neurons in the SN and striatum. We found that MPTP treatment dramatically decreased Nissl-positive cells in the SN. Interestingly, both ROF and rolipram reversed the effect of MPTP and increased the number of neurons in this area (Figure 7A and B). We then explored the effects of MPTP and ROF on the number of dopaminergic neuron bodies. As shown in Figure 7C–E, MPTP induced a significant loss of TH-positive neurons in the SN. In contrast, treatment with ROF markedly reduced the MPTP-induced loss of TH-positive cells. Rolipram exhibited a similar effect to that of ROF. The expression of TH in mice treated with MPTP was lower compared with that in mice treated with vehicle. As expected, both ROF and rolipram increased the level of TH

significantly (Figure 7F and G).

In addition to SN, we also examined the loss of dopaminergic neuron fibers in the striatum. We found that ROF increased the number of Nissl-positive neurons (Figure 8A and B) and TH-positive dopaminergic neuron fibers (Figure 8C–E) in the striatum. Additionally, ROF enhanced the protein expression of TH in the striatum (Figure 8F–G). These results indicate that ROF improved the dopaminergic neuronal survival in the context of MPTP-induced PD in mice.

ROF promotes the phosphorylation of CREB and expression of PGC-1 α in both the SN and striatum in MPTP-treated mice

We next investigated the levels of phosphorylated CREB and PGC-1 α in the brains of MPTP-challenged mice. Dopaminergic neuron bodies were identified by TH co-labeling, and all type of cells in the SN were stained with Hoechst (Fig. 9A). A significant decrease in PGC-1 α immunofluorescence was observed in the SN of mice treated with MPTP compared with that of the control SN. PGC-1 α and TH staining were dramatically increased after treatment with ROF or rolipram (Figure 9A). These results were consistent with the data that the protein level of PGC-1 α was increased significantly in mice administrated with ROF (Figure 9B). Consistently, ROF treatment dramatically increased the fluorescence of p-CREB compared with that of mice only treated with MPTP (Figure 9C). Western blotting analysis also showed that the phosphorylation of CREB in ROF-treated mice was significantly enhanced compared to that in mice only treated with MPTP (Figure 9D). The changes in p-CREB and PGC-1 α in the striatum were similar to those of in the SN. ROF treatment increased the protein expression of PGC-1 α in the striatum (Figure 10A–B). Additionally, the phosphorylation of CREB was enhanced significantly (Figure 10C–D). In addition, ROF significantly enhanced the level of ATP in the SN of mice subjected to MPTP (Supplementary Figure S5). The above data suggest that ROF exerted a neuroprotective effect accompanied by upregulation of PGC-1 α and p-CREB in an MPTP-induced mouse model of PD.

Discussion

The major finding of the current study is that inhibition of PDE4 by ROF protects

dopaminergic neurons against apoptosis in models of PD. Interestingly, we also noticed that MPP⁺ treatment resulted in nuclear accumulation of cleaved caspase-3, while ROF reversed the effect of MPP⁺ (Fig.S1). It was proposed that the nuclear translocation of caspase-3 is mediated by an active transport way (Kamada *et al.*, 2005). Activated caspase-3 cleaves its nuclear substrates, resulting in DNA fragmentation and chromatin condensation (Luo *et al.*, 2010). Our data suggested that ROF is effective to block the pro-apoptotic role of MPP⁺ in dopaminergic neurons. As a selective inhibitor of PDE4, the protective effect of ROF against PD has never been reported previously. In view of the many advantages of ROF over the currently available PDE4 inhibitors, we were interested in investigating the protective role of ROF in PD models. First, compared with that of the first-generation PDE4 inhibitor rolipram, ROF exhibits a higher inhibitory effect on PDE4. ROF exhibits lower IC₅₀ values (56.2 nM) against PDE4CAT (core catalytic domains of human PDE4) compared with that of rolipram (2480 nM). In addition, ROF also shows nanomolar IC₅₀ values against PDE4A (31 nM), PDE4B (42.9 nM), and PDE4D (11.8 nM) (Guo *et al.*, 2017), indicating that ROF is a potent PDE4 inhibitor. Second, compared with roflumilast, ROF crosses the blood brain barrier easily (Guo *et al.*, 2017), which makes it possible to develop ROF as a candidate drug for the treatment of neurological disorders. Under BBB penetration, ROF has less or no emetic potential compared with that of canonical PDE4 inhibitors (Guo *et al.*, 2017). Finally, ROF is effective in improving cognition in APP/PS1 mice (Guo *et al.*, 2017). Importantly, PD is accompanied by non-motor dysfunctions, including cognitive deficits. Hence, we hypothesized that ROF may ameliorate cognitive deficits in PD. Additionally, inhibition of inflammation is beneficial for the amelioration of PD symptoms (Kim *et al.*, 2018). Our previous studies have shown that ROF is effective in decreasing the production of IL-1 β and TNF- α (Guo *et al.*, 2017; You *et al.*, 2017). What's more, our recent studies indicated that ROF promotes autophagy in neuronal cells (You *et al.*, 2017). Appropriate autophagy is helpful to clean out damaged cells and toxins, which is also beneficial for neuronal survival. Hence, we also predicted that PD patients would benefit from both the anti-inflammatory and autophagy-enhancing effects of ROF.

Mitochondrial dysfunction plays an important role in the progression of PD (Burbulla *et al.*, 2017; Scholpa *et al.*, 2018). Damaged mitochondria can negatively affect the physiological

functions of neurons. For example, impaired mitochondria produce excessive ROS that can destroy the cell membrane and nuclear membrane (Hedde *et al.*, 2017). Mitochondria also influence calcium homeostasis inside and outside of cells, which directly affects neuronal functions (Surmeier, 2018). In addition, impaired mitochondria produce less ATP, which will subsequently create problems with axonal transport and neurotransmission (Smith *et al.*, 2018). All of these aspects can affect the survival and functions of dopamine-producing neurons, and, thus contribute to the development of PD. In our previous studies, we found that inhibition of PDE4 in SH-SY5Y cells could counteract the decrease of MMP induced by MPP⁺ (Zhong *et al.*, 2018). We also found that inhibition of intracellular PDE4 activity in neurons increased the production of ATP under the condition of oxygen-glucose deprivation (Xu *et al.*, 2019). These findings drew our attention to the regulation of mitochondrial function by PDE4. Our results showed that inhibition of PDE4 ameliorated mitochondrial morphology (Figure 2). Several possible biological functions of mitochondrial networks and mitochondrial footprints have been proposed, such as improved quality control, an increased ATP synthesis rate and protection against apoptotic stressors (Hoitzing *et al.*, 2015; Briston *et al.*, 2018). These morphological changes were paralleled with improved biological functions of mitochondria, including increased OCR, mtDNA, MMP, and ATP production (Figure 2). We would like to point out that IC₅₀ value of ROF is 56.2 nM (Guo *et al.*, 2017), while in the present study, the neuroprotective effects of ROF was observe at the dose of 20 μM, which is relatively high considering that the IC₅₀ value is in the nanomolar range. The detailed mechanisms are deserved to be studied in future. Probably, the influences of PDE4 inhibition on the activities of other PDE family members, especially PDE7 and PDE8, are helpful to answer the question.

We then investigated the potential mechanisms of ROF protection. PGC-1α is highly expressed in neuronal cells (Canto *et al.*, 2009). Physiologically, PGC-1α functions as a regulator in mediating mitochondria biogenesis, ATP production and mitophagy, thereby maintaining the normal biological functions of mitochondria (Johri *et al.*, 2013). Interestingly, inhibition of PDE4 increases cAMP levels in neurons, thereby activating the PKA/CREB signaling pathway (Richter *et al.*, 2013). Of note, the promoter of PGC-1α contains the binding site of CREB (the sequence is TGACGTCA) (Fernandez-Marcos *et al.*, 2011). CREB

phosphorylation increases the transcription of PGC-1 α (Wu *et al.*, 2006). Activation of the CREB-PGC-1 α signaling in dopaminergic neurons contributes to an increased cell viability, and thus CREB-PGC-1 α pathway has been proposed as a promising therapeutic target for the treatment of PD (Makela *et al.*, 2016; Kang *et al.*, 2017). These findings are consistent with data obtained in the present studies. ROF was found to induce the activation of CREB, as was evident by the increase in the phosphorylation of CREB at Ser133 (Figure 3C and D). In addition to CREB, we also found that the protein expression of PGC-1 α was increased as well (Figure 3E and F). Interestingly, Figure 1C, 1E and 1F showed that 20 μ M ROF exerted around 10% cytoprotection, while ROF produced much higher restoration of the levels of phosphorylated CREB and PGC-1 α . This observation suggests that inhibition of CREB/PGC-1 α pathway is not the sole machinery which destroys neuronal cells by MPP⁺. MPP⁺ is a potent neurotoxin destroying dopaminergic neurons through multiple pathways. For example, MPP⁺ has been shown to induce neurotoxicity by promoting an overload of misfolded proteins in PD (Lehtonen *et al.*, 2016). MPP⁺ may also induce neuronal injury through up-regulating the expression of cation channels (Sun *et al.*, 2018). In this study, we verified that ROF was capable of activating CREB/PGC-1 α pathway in neuronal cells treated with MPP⁺, but these effects are insufficient to totally block the toxicity induced by MPP⁺. Combination of ROF with other neuroprotective agents may serve the purpose. To further verify the involvement of PKA/CREB, we then employed the PKA inhibitor H-89 to block the activation of CREB mediated by cAMP/PKA and to verify the regulation of CREB on the expression of PGC-1 α (Figure 4A–C). The results showed that H-89 decreased both the phosphorylation of CREB and the expression of PGC-1 α , indicating that PGC-1 α was regulated by PKA/CREB. In accordance with these findings, H-89 and PGC-1 α siRNA blocked the reduction of both MMP and cell viability. Hence, ROF mediated its protective effect through activating the PKA/CREB/PGC-1 α signaling pathway. Most importantly, ROF shows similar neuroprotection in human dopaminergic neurons as that in SH-SY5Y cells (Figure 5). These findings further support the conclusion that ROF confers neuroprotection against MPP⁺-triggered neuronal cell death insult.

Consistent with these *in vitro* data, treatment with ROF in mice challenged with MPTP improved motor behavioral performance and decreased the loss of dopaminergic neurons

induced by MPTP. Importantly, the phosphorylation of CREB and expression of PGC-1 α were enhanced by ROF in both the SN and striatum. These findings support the hypothesis that PDE4 might be a potential target for PD treatment, and that CREB/PGC-1 α is involved in the protective effect of ROF. It is noteworthy that PGC-1 α regulates mitochondrial production and functions in several ways. For example, PGC-1 α is involved in mitophagy (Yeo *et al.*, 2019). Appropriate autophagy is beneficial for the survival of dopaminergic neurons (Hu *et al.*, 2017). Our present study mainly focused on the regulation of PDE4 inhibition on CREB/PGC-1 α and its role in neuroprotection against MPP⁺/MPTP. Further studies are needed in the future to determine the involvement the mitochondrial biogenesis and autophagy in the protective effect of ROF.

In conclusion, our results revealed that ROF prevented MPP⁺/MPTP-induced degeneration of dopaminergic neurons, ameliorated motor dysfunctions, increased TH expression, and restored mitochondrial function. These findings indicate that ROF is probably a promising drug candidate for treating PD. Further research and preclinical studies are needed to systematically investigate the potential of ROF for the treatment of PD.

Acknowledgments:

This work was supported by National Natural Science Foundation of China (No. 81773698), the Program for Changjiang Scholars and Innovative Research Team in University (IRT_16R37), Science and Technology Program of Guangdong (Nos. 2018B030334001 and 2015B020211007), Science and Technology Program of Guangzhou (No. 201604020112).

Author contribution

JZ, WD, YQ, JX (Jinfeng Xie) and JX (Jiao Xiao) performed the experiments and analyzed the data. JZ, HW and JP drafted the manuscript. HW and JP designed research project, supervised experiments and critically reviewed the manuscript. All authors have given their final approval for the manuscript.

Conflict of interest

The authors declare that they have no conflict of interest.

Declaration of transparency and scientific rigour

This Declaration acknowledges that this paper adheres to the principles for transparent reporting and scientific rigour of preclinical research as stated in the BJP guidelines for Design & Analysis, Immunoblotting and Immunochemistry, and Animal Experimentation, and as recommended by funding agencies, publishers and other organizations engaged with supporting research.

References

Alexander SP, Christopoulos A, Davenport AP, Kelly E, Marrion NV, Peters JA, *et al.* (2017). THE CONCISE GUIDE TO PHARMACOLOGY 2017/18: G protein-coupled receptors. *British journal of pharmacology* **174** Suppl 1: S17-S129.

Amende I, Kale A, McCue S, Glazier S, Morgan JP, Hampton TG (2005). Gait dynamics in mouse models of Parkinson's disease and Huntington's disease. *Journal of neuroengineering and rehabilitation* **2**: 20.

Briston T, Stephen JM, Thomas LW, Esposito C, Chung YL, Syafruddin SE, *et al.* (2018). VHL-Mediated Regulation of CHCHD4 and Mitochondrial Function. *Frontiers in oncology* **8**: 388.

Burbulla LF, Song P, Mazzulli JR, Zampese E, Wong YC, Jeon S, *et al.* (2017). Dopamine oxidation mediates mitochondrial and lysosomal dysfunction in Parkinson's disease. *Science* **357**(6357): 1255-1261.

Canto C, Auwerx J (2009). PGC-1alpha, SIRT1 and AMPK, an energy sensing network that controls energy expenditure. *Current opinion in lipidology* **20**(2): 98-105.

Ciron C, Zheng L, Bobela W, Knott GW, Leone TC, Kelly DP, *et al.* (2015). PGC-1alpha activity in nigral dopamine neurons determines vulnerability to alpha-synuclein. *Acta neuropathologica communications* **3**: 16.

Curtis MJ, Alexander S, Cirino G, Docherty JR, George CH, Giembycz MA, *et al.* (2018). Experimental design and analysis and their reporting II: updated and simplified guidance for authors and peer reviewers. *British journal of pharmacology* **175**(7): 987-993.

Dauer W, Przedborski S (2003). Parkinson's disease: mechanisms and models. *Neuron* **39**(6): 889-909.

Dyke HJ, Montana JG (2002). Update on the therapeutic potential of PDE4 inhibitors. *Expert opinion on investigational drugs* **11**(1): 1-13.

Fernandez-Marcos PJ, Auwerx J (2011). Regulation of PGC-1alpha, a nodal regulator of mitochondrial biogenesis. *The American journal of clinical nutrition* **93**(4): 884S-890.

Goldberg NR, Hampton T, McCue S, Kale A, Meshul CK (2011). Profiling changes in gait dynamics resulting from

progressive 1-methyl-4-phenyl-1,2,3,6-tetrahydropyridine-induced nigrostriatal lesioning. *Journal of neuroscience research* **89**(10): 1698-1706.

Guo H, Cheng Y, Wang C, Wu J, Zou Z, Niu B, *et al.* (2017). FFPM, a PDE4 inhibitor, reverses learning and memory deficits in APP/PS1 transgenic mice via cAMP/PKA/CREB signaling and anti-inflammatory effects. *Neuropharmacology* **116**: 260-269.

Harding SD, Sharman JL, Faccenda E, Southan C, Pawson AJ, Ireland S, *et al.* (2018). The IUPHAR/BPS Guide to PHARMACOLOGY in 2018: updates and expansion to encompass the new guide to IMMUNOPHARMACOLOGY. *Nucleic acids research* **46**(D1): D1091-D1106.

Hedde JR, Hanks AN, Schmidt CJ, Hughes ZA (2017). The isozyme selective phosphodiesterase-4 inhibitor, ABI-4, attenuates the effects of lipopolysaccharide in human cells and rodent models of peripheral and CNS inflammation. *Brain, behavior, and immunity* **64**: 285-295.

Heikkila RE, Hess A, Duvoisin RC (1984). Dopaminergic neurotoxicity of 1-methyl-4-phenyl-1,2,5,6-tetrahydropyridine in mice. *Science* **224**(4656): 1451-1453.

Herzig S, Long F, Jhala US, Hedrick S, Quinn R, Bauer A, *et al.* (2001). CREB regulates hepatic gluconeogenesis through the coactivator PGC-1. *Nature* **413**(6852): 179-183.

Hoitzing H, Johnston IG, Jones NS (2015). What is the function of mitochondrial networks? A theoretical assessment of hypotheses and proposal for future research. *BioEssays : news and reviews in molecular, cellular and developmental biology* **37**(6): 687-700.

Hu ZY, Chen B, Zhang JP, Ma YY (2017). Up-regulation of autophagy-related gene 5 (ATG5) protects dopaminergic neurons in a zebrafish model of Parkinson's disease. *The Journal of biological chemistry* **292**(44): 18062-18074.

Jankovic J (2008). Parkinson's disease: clinical features and diagnosis. *Journal of neurology, neurosurgery, and psychiatry* **79**(4): 368-376.

Johri A, Chandra A, Flint Beal M (2013). PGC-1alpha, mitochondrial dysfunction, and Huntington's disease. *Free radical biology & medicine* **62**: 37-46.

Kamada S, Kikkawa U, Tsujimoto Y, Hunter T (2005). Nuclear translocation of caspase-3 is dependent on its proteolytic activation and recognition of a substrate-like protein(s). *The Journal of biological chemistry* **280**(2): 857-860.

Kang H, Khang R, Ham S, Jeong GR, Kim H, Jo M, *et al.* (2017). Activation of the ATF2/CREB-PGC-1alpha pathway by metformin leads to dopaminergic neuroprotection. *Oncotarget* **8**(30): 48603-48618.

Kilkenny C, Browne W, Cuthill IC, Emerson M, Altman DG, Group NCRGW (2010). Animal research: reporting in vivo experiments: the ARRIVE guidelines. *British journal of pharmacology* **160**(7): 1577-1579.

Kim HW, Lee HS, Kang JM, Bae SH, Kim C, Lee SH, *et al.* (2018). Dual Effects of Human Placenta-Derived Neural Cells on Neuroprotection and the Inhibition of Neuroinflammation in a Rodent Model of Parkinson's Disease. *Cell transplantation* **27**(5): 814-830.

Kostrzewa RM, Kostrzewa JP, Brus R (2002). Neuroprotective and neurotoxic roles of levodopa (L-DOPA) in neurodegenerative disorders relating to Parkinson's disease. *Amino acids* **23**(1-3): 57-63.

Krug AK, Gutbier S, Zhao L, Poltl D, Kullmann C, Ivanova V, *et al.* (2014). Transcriptional and metabolic adaptation of human neurons to the mitochondrial toxicant MPP(+). *Cell death & disease* **5**: e1222.

Lehtonen S, Jaronen M, Vehvilainen P, Lakso M, Rudgalvyte M, Keksa-Goldsteine V, *et al.* (2016). Inhibition of Excessive Oxidative Protein Folding Is Protective in MPP(+) Toxicity-Induced Parkinson's Disease Models. *Antioxidants & redox signaling* **25**(8): 485-497.

Luo M, Lu Z, Sun H, Yuan K, Zhang Q, Meng S, *et al.* (2010). Nuclear entry of active caspase-3 is facilitated by its p3-recognition-based specific cleavage activity. *Cell research* **20**(2): 211-222.

Makela J, Tselykh TV, Kukkonen JP, Eriksson O, Korhonen LT, Lindholm D (2016). Peroxisome proliferator-activated receptor-gamma (PPARGgamma) agonist is neuroprotective and stimulates PGC-1alpha expression and CREB phosphorylation in human dopaminergic neurons. *Neuropharmacology* **102**: 266-275.

McGrath JC, Lilley E (2015). Implementing guidelines on reporting research using animals (ARRIVE etc.): new requirements for publication in BJP. *British journal of pharmacology* **172**(13): 3189-3193.

Migdalska-Richards A, Schapira AH (2016). The relationship between glucocerebrosidase mutations and Parkinson disease. *Journal of neurochemistry* **139 Suppl 1**: 77-90.

Mudo G, Makela J, Di Liberto V, Tselykh TV, Olivieri M, Piepponen P, *et al.* (2012). Transgenic expression and activation of PGC-1alpha protect dopaminergic neurons in the MPTP mouse model of Parkinson's disease. *Cellular and molecular life sciences : CMLS* **69**(7): 1153-1165.

Niccolini F, Wilson H, Pagano G, Coello C, Mehta MA, Searle GE, *et al.* (2017). Loss of phosphodiesterase 4 in Parkinson disease: Relevance to cognitive deficits. *Neurology* **89**(6): 586-593.

Picconi B, Hernandez LF, Obeso JA, Calabresi P (2018). Motor complications in Parkinson's disease: Striatal molecular and electrophysiological mechanisms of dyskinesias. *Movement disorders : official journal of the Movement Disorder Society* **33**(6): 867-876.

Richter W, Menniti FS, Zhang HT, Conti M (2013). PDE4 as a target for cognition enhancement. *Expert opinion on therapeutic targets* **17**(9): 1011-1027.

Schildknecht S, Karreman C, Poltl D, Efremova L, Kullmann C, Gutbier S, *et al.* (2013). Generation of genetically-modified human differentiated cells for toxicological tests and the study of neurodegenerative

diseases. *Altx* **30**(4): 427-444.

Scholpa NE, Lynn MK, Corum D, Boger HA, Schnellmann RG (2018). 5-HT1F receptor-mediated mitochondrial biogenesis for the treatment of Parkinson's disease. *British journal of pharmacology* **175**(2): 348-358.

Scholz D, Poltl D, Genewsky A, Weng M, Waldmann T, Schildknecht S, *et al.* (2011). Rapid, complete and large-scale generation of post-mitotic neurons from the human LUHMES cell line. *Journal of neurochemistry* **119**(5): 957-971.

Smith GM, Gallo G (2018). The role of mitochondria in axon development and regeneration. *Developmental neurobiology* **78**(3): 221-237.

St-Pierre J, Drori S, Uldry M, Silvaggi JM, Rhee J, Jager S, *et al.* (2006). Suppression of reactive oxygen species and neurodegeneration by the PGC-1 transcriptional coactivators. *Cell* **127**(2): 397-408.

Stocchi F, Torti M, Fossati C (2016). Advances in dopamine receptor agonists for the treatment of Parkinson's disease. *Expert opinion on pharmacotherapy* **17**(14): 1889-1902.

Sun Y, Sukumaran P, Selvaraj S, Cilz NI, Schaar A, Lei S, *et al.* (2018). TRPM2 Promotes Neurotoxin MPP(+)/MPTP-Induced Cell Death. *Molecular neurobiology* **55**(1): 409-420.

Surmeier DJ (2018). Determinants of dopaminergic neuron loss in Parkinson's disease. *The FEBS journal* **285**(19): 3657-3668.

Tomkova S, Misuth M, Lenkavska L, Miskovsky P, Huntosova V (2018). In vitro identification of mitochondrial oxidative stress production by time-resolved fluorescence imaging of glioma cells. *Biochimica et biophysica acta. Molecular cell research* **1865**(4): 616-628.

Valente AJ, Maddalena LA, Robb EL, Moradi F, Stuart JA (2017). A simple ImageJ macro tool for analyzing mitochondrial network morphology in mammalian cell culture. *Acta histochemica* **119**(3): 315-326.

Wu Z, Huang X, Feng Y, Handschin C, Feng Y, Gullicksen PS, *et al.* (2006). Transducer of regulated CREB-binding proteins (TORCs) induce PGC-1alpha transcription and mitochondrial biogenesis in muscle cells. *Proceedings of the National Academy of Sciences of the United States of America* **103**(39): 14379-14384.

Xu B, Wang T, Xiao J, Dong W, Wen HZ, Wang X, *et al.* (2019). FCPR03, a novel phosphodiesterase 4 inhibitor, alleviates cerebral ischemia/reperfusion injury through activation of the AKT/GSK3beta/ beta-catenin signaling pathway. *Biochemical pharmacology* **163**: 234-249.

Yang L, Calingasan NY, Lorenzo BJ, Beal MF (2008). Attenuation of MPTP neurotoxicity by rolipram, a specific inhibitor of phosphodiesterase IV. *Experimental neurology* **211**(1): 311-314.

Yeo D, Kang C, Gomez-Cabrera MC, Vina J, Ji LL (2019). Intensified mitophagy in skeletal muscle with aging is downregulated by PGC-1alpha overexpression in vivo. *Free radical biology & medicine* **130**: 361-368.

You T, Cheng Y, Zhong J, Bi B, Zeng B, Zheng W, *et al.* (2017). Roflupram, a Phosphodiesterase 4 Inhibitor, Suppresses Inflammasome Activation through Autophagy in Microglial Cells. *ACS chemical neuroscience* **8**(11): 2381-2392.

Zheng S, Kaur G, Wang H, Li M, Macnaughtan M, Yang X, *et al.* (2008). Design, synthesis, and structure-activity relationship, molecular modeling, and NMR studies of a series of phenyl alkyl ketones as highly potent and selective phosphodiesterase-4 inhibitors. *Journal of medicinal chemistry* **51**(24): 7673-7688.

Zhong J, Xie J, Xiao J, Li D, Xu B, Wang X, *et al.* (2019). Inhibition of PDE4 by FCPR16 induces AMPK-dependent autophagy and confers neuroprotection in SH-SY5Y cells and neurons exposed to MPP(+)-induced oxidative insult. *Free radical biology & medicine* **135**: 87-101.

Zhong J, Yu H, Huang C, Zhong Q, Chen Y, Xie J, *et al.* (2018). Inhibition of phosphodiesterase 4 by FCPR16 protects SH-SY5Y cells against MPP(+)-induced decline of mitochondrial membrane potential and oxidative stress. *Redox biology* **16**: 47-58.

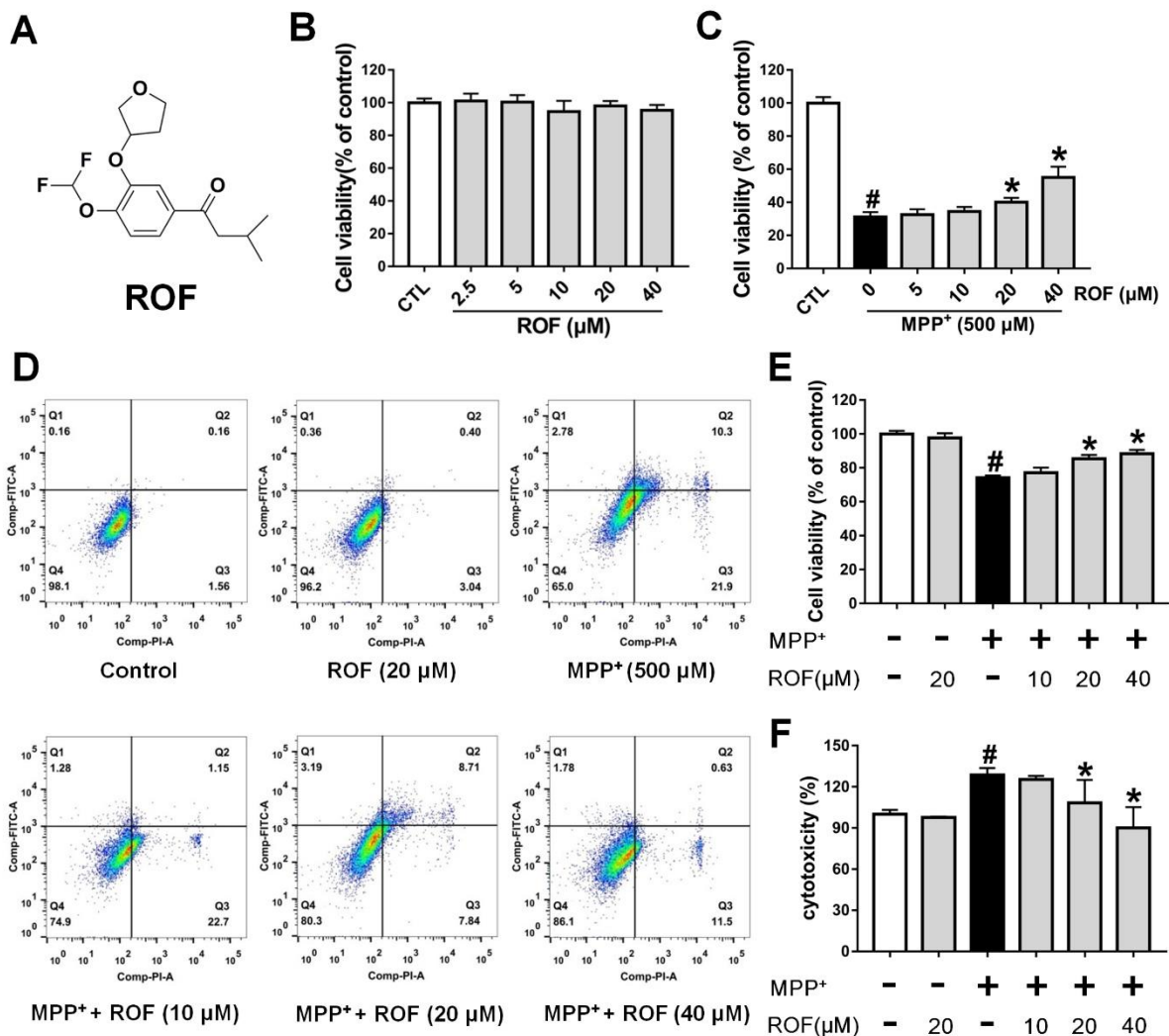


Fig. 1. ROF increases cell viability of MPP⁺-induced cells. (A) The chemical structure of Roflupram (ROF). (B) SH-SY5Y cells were treated with various concentrations of ROF for 48 h to evaluate the cytotoxic effects on cells. (C) Cells were pretreated with different concentrations of ROF for 1 h, and then treated with 500 μM of MPP⁺ for 48 h to measure cell viability with MTT assay. (D,E) Cells were pretreated with various concentrations of ROF 1 h earlier, and were then exposed to 500 μM of MPP⁺ for 24 h, cell viability was measured using flow cytometry. Representative graphs of flow cytometric outputs for each group are shown in (D), and statistical analysis of flow cytometry is presented in (E). (F) Cells were treated with various concentrations of ROF in advance, and were then stimulated with 500 μM of MPP⁺ for 48 h to measure LDH activity in the medium. Data are presented as mean ± SD (n = 5) and represent five independent experiments. #*P* < 0.05 versus control group. **P* < 0.05 versus MPP⁺-treated group.

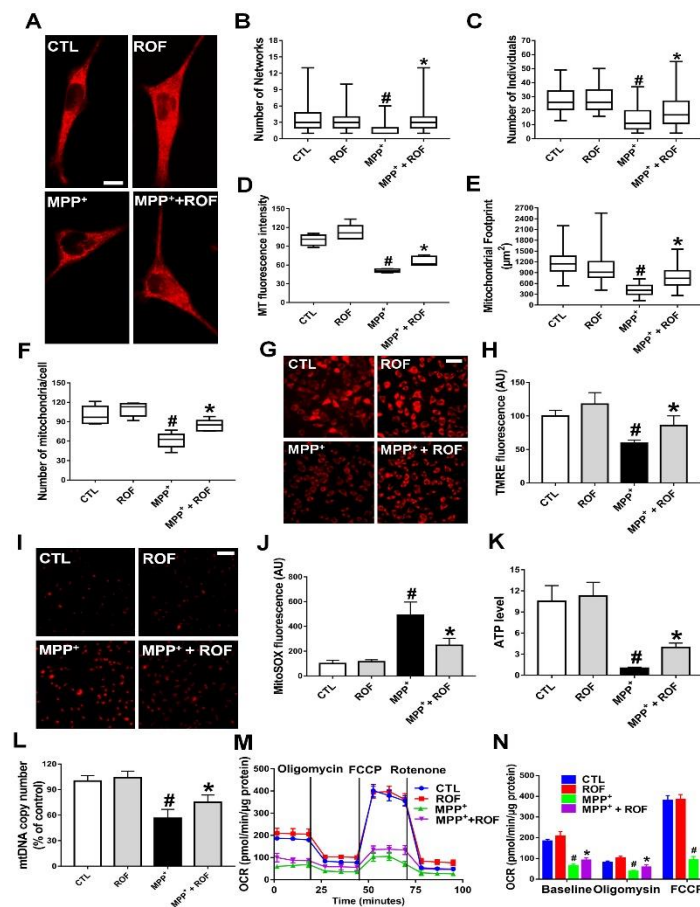


Fig. 2. Effect of ROF on mitochondrial morphology and function of MPP⁺-treated cells. (A) SH-SY5Y cells were pretreated with ROF (20 μ M) for 1 h, and were then treated with 500 μ M of MPP⁺ for 24 h. Mitotracker Red was added to mark mitochondria. Scale bar = 10 μ m. Statistical analysis was performed on 100 cells in each group to obtain five data sets; the number of networks (B), number of individuals (C), MT fluorescence intensity (D), mitochondrial footprint (E) and the number of mitochondria per cell (F). After treating cells with ROF for 1 h in advance, 500 μ M of MPP⁺ was added for 24 h to measure mitochondrial membrane potential (MMP) (G) and oxidative stress (I), and statistical analyses were determined via TMRE fluorescence (H) and MitoSOX fluorescence (J). (K) Cells were pretreated with ROF (20 μ M) for 1 h, and then treated with 500 μ M of MPP⁺ for 24 h. ATP levels were detected with an ATP Assay kit. (L) mtDNA copy number was measured in SH-SY5Y cells by real-time PCR. (M) Oxygen consumption rate (OCR) was measured in SH-SY5Y cells using the Seahorse XF-24 Analyzer in response to the sequential administration of oligomycin (1 μ M), FCCP (0.5 μ M) and rotenone (2 μ M). (N) Quantification of OCR in panel (M). Scale bar = 500 μ m. Data are presented as mean \pm SD (n = 5) and represent five independent experiments. #*P* < 0.05 versus control group. **P* < 0.05 versus MPP⁺-treated group.

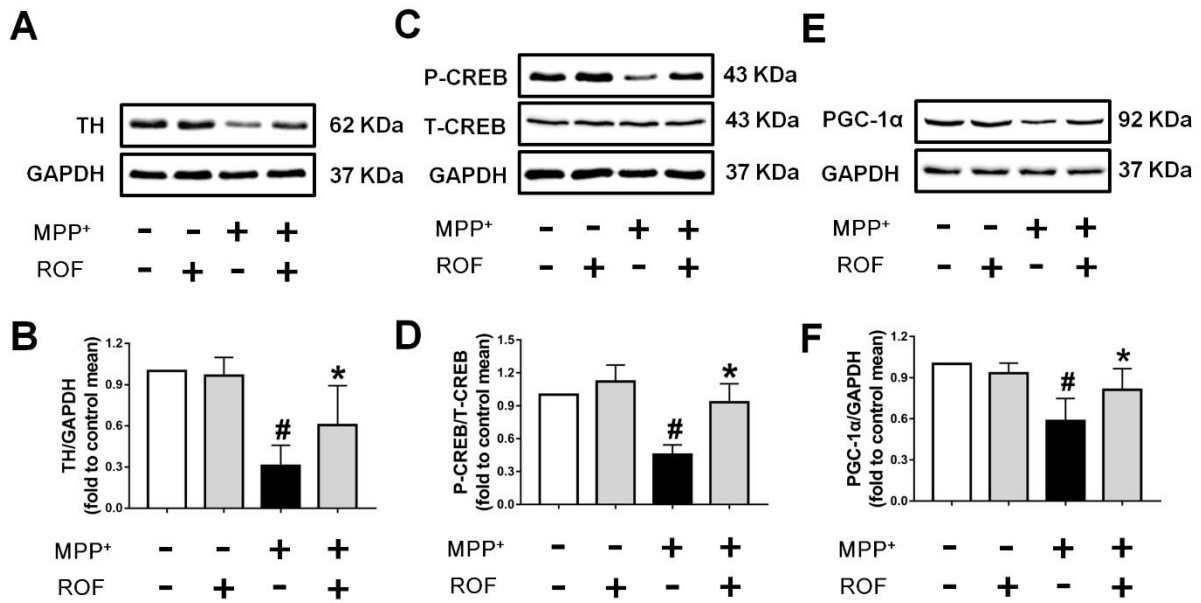


Fig. 3. Effect of ROF on the expression of related proteins of MPP⁺-treated cells. SH-SY5Y cells were pretreated with ROF (20 μM) for 1 h, and then treated with 500 μM of MPP⁺ for 24 h. After cells were processed, the expression levels of TH (A), p- CREB (C), PGC-1α (E) were detected by Western blotting. (B) Densitometric quantification of TH/GAPDH in (A). (D) Densitometric quantification of p-CREB/T-CREB in (C). (F) Densitometric quantification PGC-1α/GAPDH in (E). Data are presented as mean ± SD (n = 5) and represent five independent experiments. [#]*P* < 0.05 versus control group. ^{*}*P* < 0.05 versus MPP⁺-treated group.

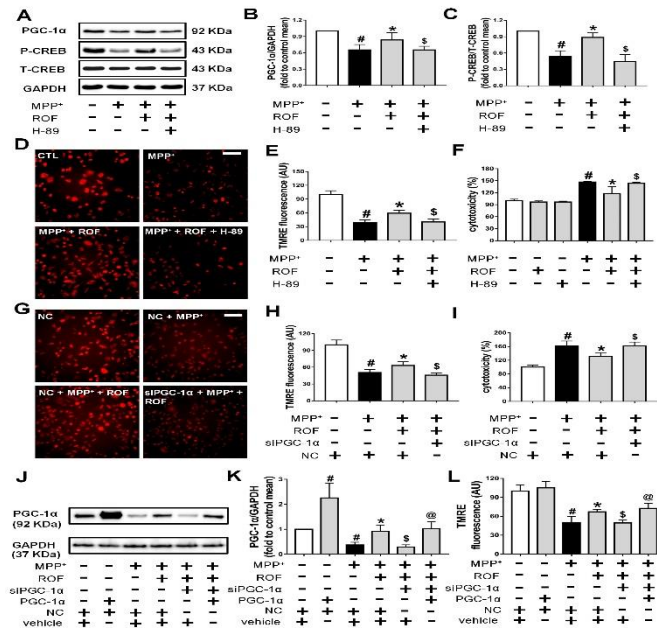


Fig. 4. The CREB-PGC-1 α pathway is involved in the protective effects of ROF in MPP⁺-treated cells. (A) SH-SY5Y cells were pretreated with H-89 (10 μ M) for 1 h, and then treated with ROF (20 μ M) for 1 h, after that, 500 μ M of MPP⁺ was added for 24 h. After cells were processed, the expression levels of PGC-1 α , p- CREB and total CREB were detected by Western blotting. (B, C) Densitometric quantification of PGC-1 α /GAPDH (B) in (A) and p-CREB/T- CREB (C) in (A). (D) Cells were pretreated with H-89 (10 μ M) for 1 h, and then treated with ROF (20 μ M) for 1 h. Subsequently, 500 μ M of MPP⁺ was added to stimulate with cells for 24 h. After treatment, cells were washed with PBS and dyed with TMRE (50 nM) for 20 min. Finally, cells were taken under a fluorescence microscope. Scale bar = 500 μ m. (E) Statistical analysis of fluorescent pictures in (D). (F) Cells were pretreated with H-89 (10 μ M) for 1 h, and then treated with ROF (20 μ M) for 1 h, after that, 500 μ M of MPP⁺ was added for 48 h. After treatment, LDH activity in the medium was measured. (G) Transfected cells were pretreated with ROF (20 μ M) for 1 h, then, 500 μ M of MPP⁺ was added for 24 h. After cells were processed, cells were dyed with TMRE (50 nM) for 20 min. Finally, cells were placed under a fluorescent microscope for imaging. Scale bar = 500 μ m. (H) Statistical analysis of fluorescent pictures in (G). (I) Transfected cells were pretreated with ROF (20 μ M) for 1 h, and 500 μ M of MPP⁺ was added for 48 h. After treatment, LDH activity in the medium was detected. (J) SH-SY5Y cells were transfected for 24 h with PGC-1 α plasmid and with PGC-1 α siRNA or random siRNA. Transfected cells were then treated with MPP⁺ for an additional 24 h. the expression levels of PGC-1 α was detected by Western blotting. (K) Densitometric quantification of PGC-1 α /GAPDH in (J). (L) After transfection and treatment with MPP⁺, cells were dyed with TMRE (50 nM) for 20 min before imaging under a fluorescent microscope. Fluorescent pictures were analyzed statistically. Data are presented as mean \pm SD (n = 5) and represent five independent experiments. #*P* < 0.05 versus control group or negative control group. **P* < 0.05 versus MPP⁺-treated group. \$*P* < 0.05 versus MPP⁺ + ROF-treated group. @*P* < 0.05 versus siPGC-1 α + MPP⁺ + ROF-treated group.

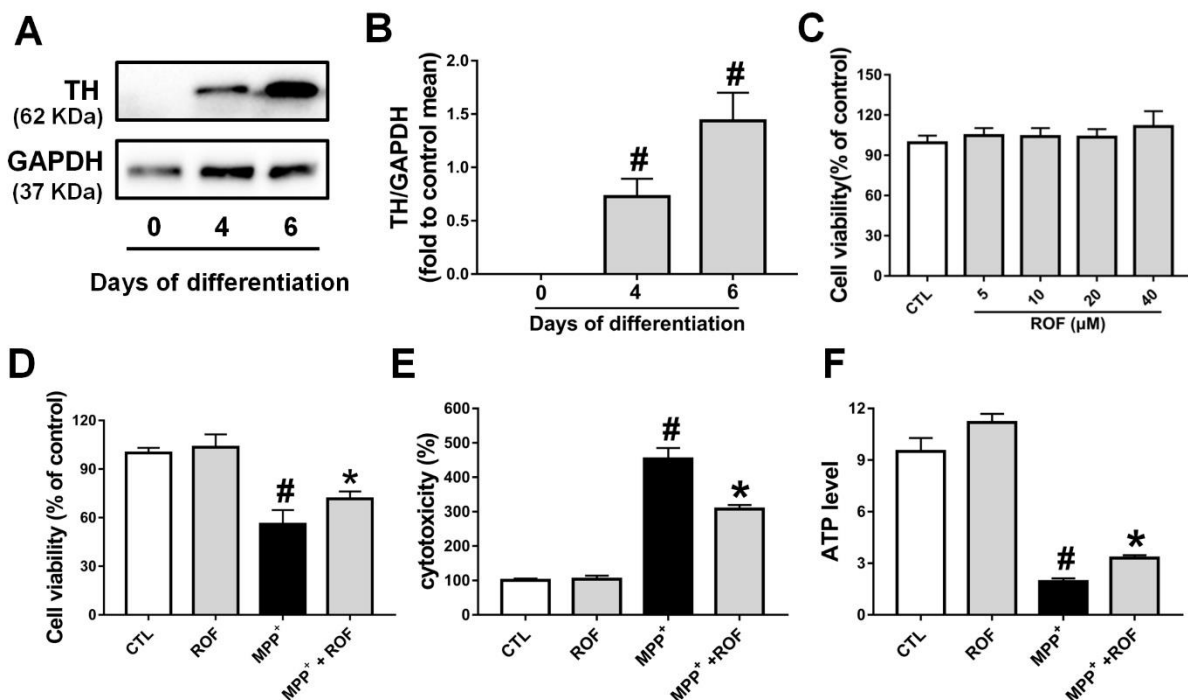


Fig. 5. The protective effects of ROF in LUHMES/MPP⁺ model. (A) Measurement of the tyrosine hydroxylase (TH) expression by Western blotting on days 0, 4 and 6 of differentiation. (B) Densitometric quantification of TH/GAPDH in (A). (C) Differentiated cells (d6) were incubated with various concentrations of ROF for 48 h, CCK-8 assay was used to evaluate the cytotoxic effects of ROF on cells. Differentiated cells (d6) were pretreated with ROF (20 μM) for 1 h, and then treated with 5 μM of MPP⁺ for an additional 48 h. After treatment, cell viability was measured by CCK-8 assay (D), LDH activity in the medium was measured by a LDH Cytotoxicity Assay Kit (E) and ATP levels were detected with an ATP Assay kit (F). Data are presented as mean \pm SD (n = 5) and represent five independent experiments. #*P* < 0.05 versus control group. **P* < 0.05 versus MPP⁺-treated group.

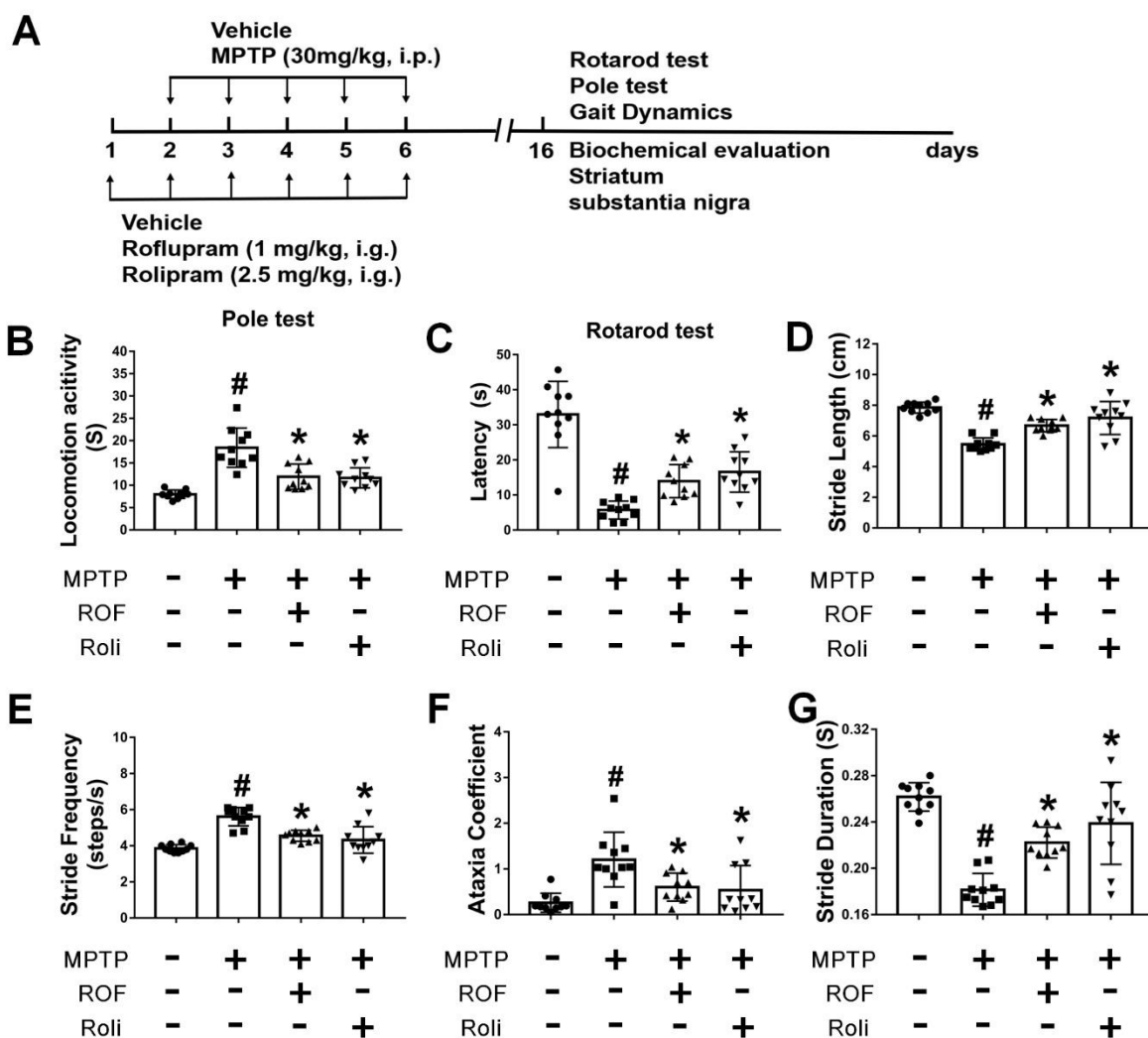


Fig. 6. Behavioral deficits of MPTP-treated mice are ameliorated via ROF and rolipram. (A) Timeline of animal experiments. (B) ROF and rolipram (Roli) ameliorated locomotor behavior in MPTP-treated mice. (C) ROF and Roli improved the performance of MPTP-treated mice in the rotarod test. The mice walked for about 5 s on a running belt at a speed of 30 cm/s. The parameters of stride length (D), stride frequency (E), ataxia coefficient (F), and stride duration (G) of the mice were obtained for statistical analysis. Gait results indicated that ROF and Roli improved limb mobility in MPTP-treated mice. Data are presented as mean \pm SD (n = 10). #*P* < 0.05 versus vehicle group. **P* < 0.05 versus MPTP-treated group.

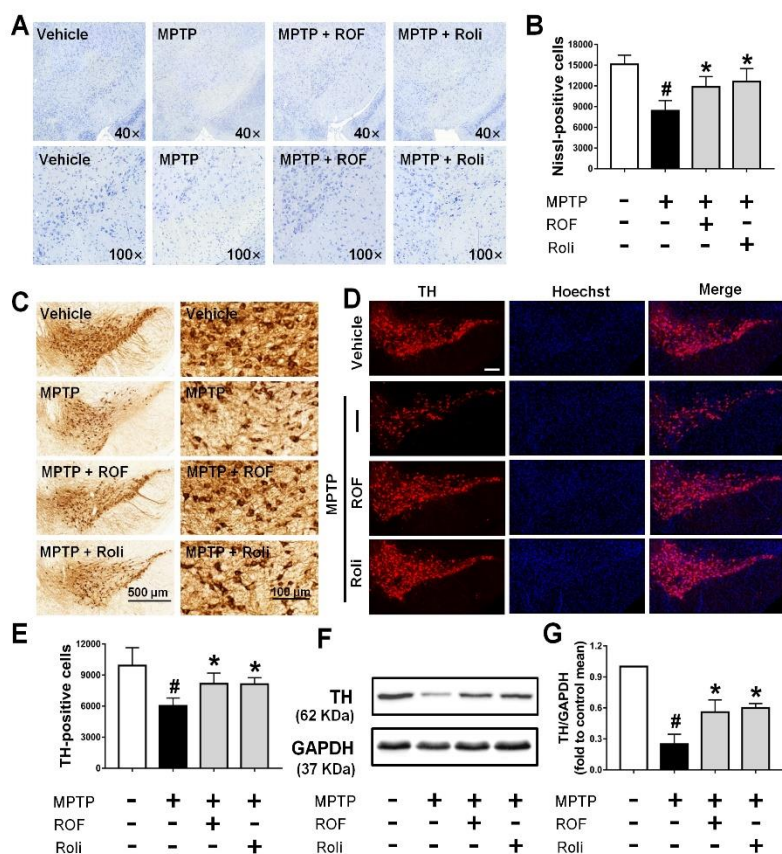


Fig. 7. ROF and rolipram reduce the loss of TH in the SN of MPTP-treated mice. (A) Nissl staining of the SN of mice in different samples under the microscope. (B) Number of Nissl-positive cells, as exhibited in (A). (C) Immunohistochemistry of the SN of mice. (E) Number of TH-positive cells, as exhibited in (C). (D) Tissue immunofluorescent staining of the SN of mice. Scale bar = 200 µm. (F) The SN of each mouse was obtained and the expression levels of TH were detected by Western blotting. (G) Densitometric quantification of TH/GAPDH in (F). Data are presented as mean ± SD (n = 5) and represent five independent experiments. #*P* < 0.05 versus vehicle group. **P* < 0.05 versus MPTP-treated group.

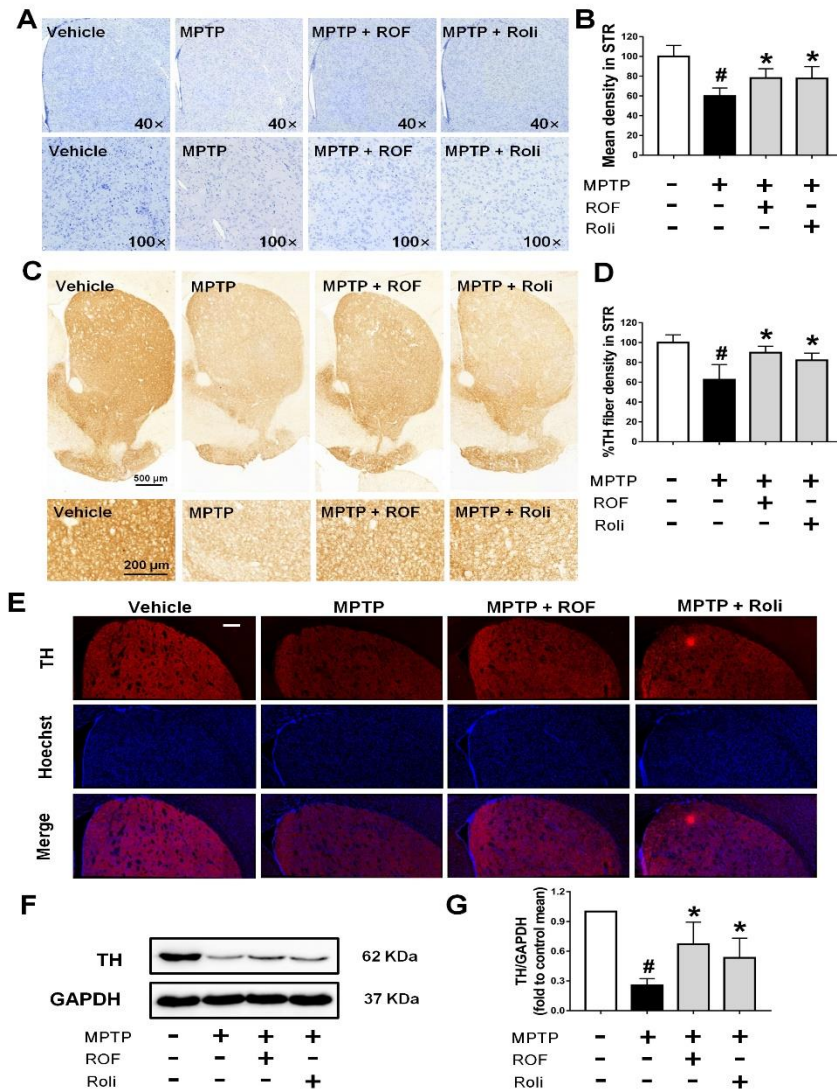


Fig. 8. ROF and rolipram reduce the loss of TH in the striatum of MPTP-treated mice. (A) Observation of Nissl staining results in the striatum in multiple samples. (B) The mean density of Nissl staining in the striatum was analyzed from samples in (A). (C) Immunohistochemistry of the striatum of mice. (D) TH fiber density in the striatum was analyzed from (C). (E) Tissue immunofluorescent staining of the striatum of mice. Scale bar = 200 μ m. (F) The striatum of each mouse was obtained and the expression levels of TH were detected by Western blotting. (G) Densitometric quantification of TH/GAPDH in (F). Data are presented as mean \pm SD (n = 5) and represent five independent experiments. # P < 0.05 versus vehicle group. * P < 0.05 versus MPTP-treated group.

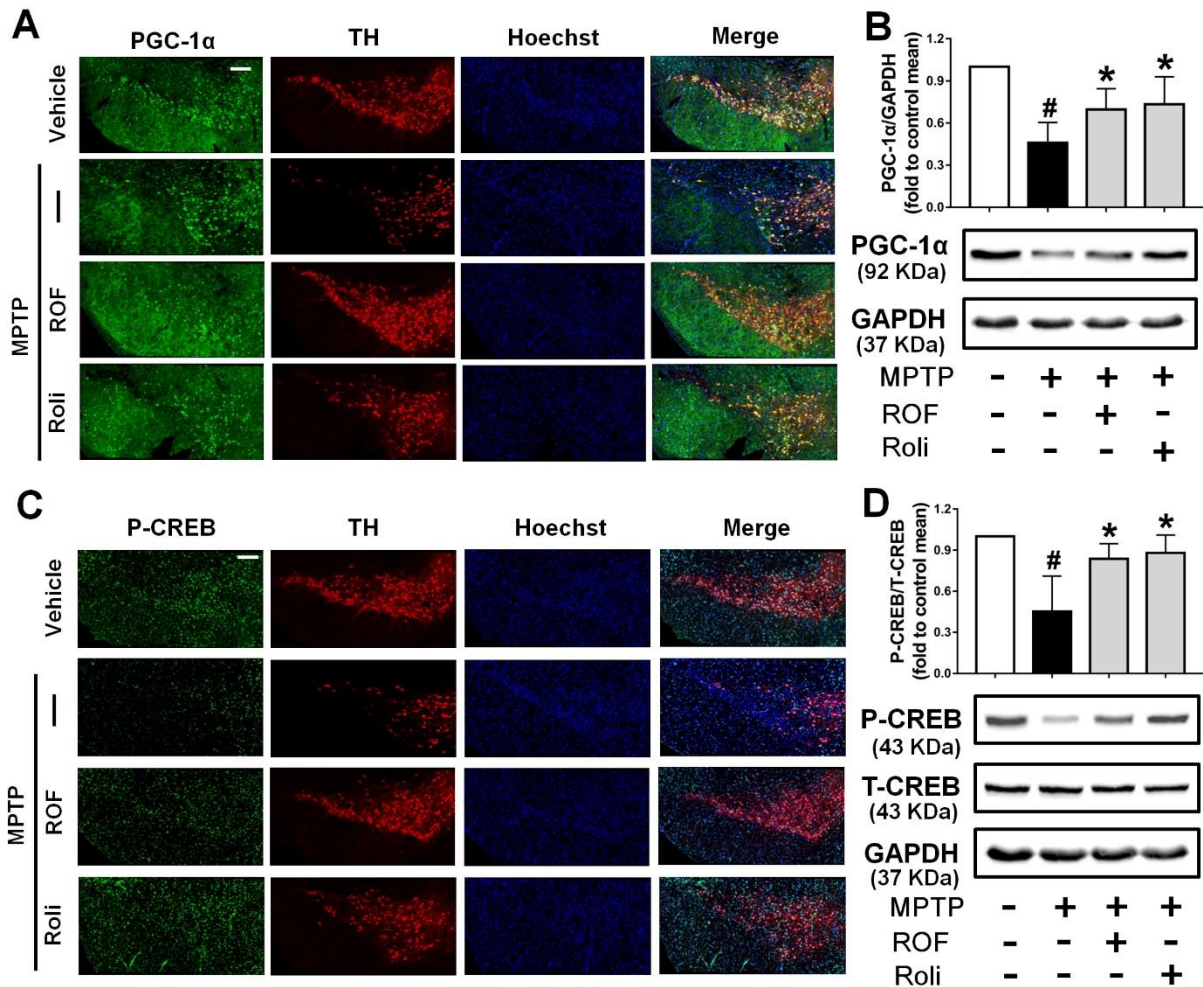


Fig. 9. ROF and rolipram regulate the CREB-PGC-1 α pathway in the SN of MPTP-treated mice. (A) Tissue immunofluorescence staining of the SN of mice was performed to detect the expression of PGC-1 α . Scale bar = 200 μ m. (B) The SN of mice were obtained and the expression levels of PGC-1 α were measured by Western blotting. (C) Tissue immunofluorescent staining of the SN of mice were carried out to measure the expression of p-CREB. Scale bar = 200 μ m. (D) SN of mice were obtained and the expression levels of p-CREB and total CREB were detected by Western blotting. Data are presented as mean \pm SD (n = 5) and represent five independent experiments. [#]*P* < 0.05 versus vehicle group. ^{*}*P* < 0.05 versus MPTP-treated group.

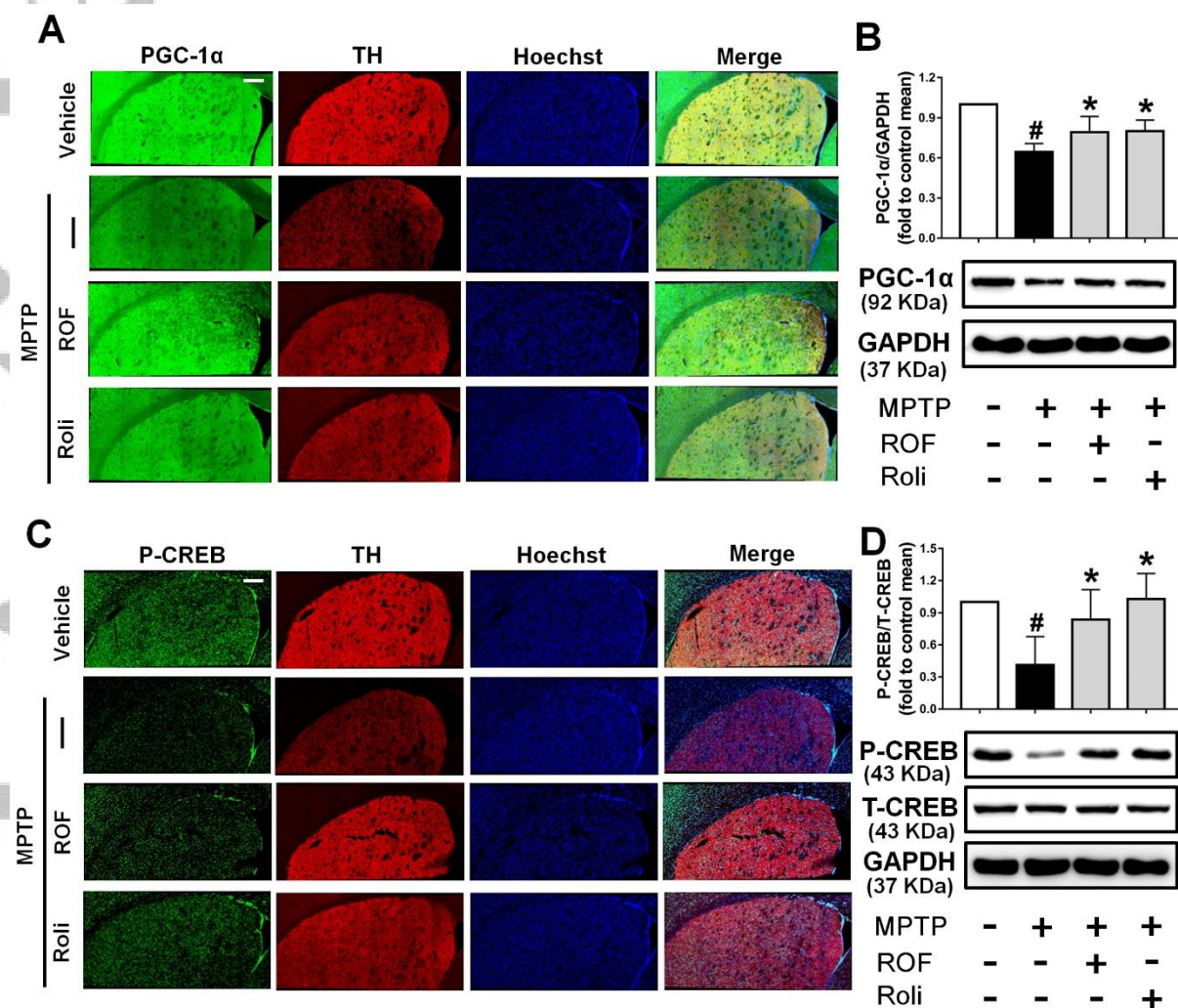


Fig. 10. ROF and rolipram regulate the CREB-PGC-1 α pathway in the striatum of MPTP-treated mice. (A) Tissue immunofluorescent staining of the striatum of mice were performed to detect the expression of PGC-1 α . Scale bar = 200 μ m. (B) The striatum of each mouse was obtained and the expression levels of PGC-1 α were measured by Western blotting. (C) Tissue immunofluorescent staining of the striatum of mice was carried out to measure the expression of p-CREB. Scale bar = 200 μ m. (D) The striatum of each mouse was obtained and the expression levels of p-CREB and total CREB were detected by Western blotting. Data are presented as mean \pm SD (n = 5) and represent five independent experiments. [#]*P* < 0.05 versus vehicle group. ^{*}*P* < 0.05 versus MPTP-treated group.